Splitting probabilities for Brownian motion with diffusing boundaries: Application to polymer translocation

Alexander K. Hartmann,[1,*] Satya N. Majumdar,[2,†] and Alberto Rosso[2,‡]

[1] *Institut für Physik, Universität Oldenburg, D-26111 Oldenburg, Germany*
[2] *LPTMS, CNRS, Univ. Paris-Sud, Université Paris-Saclay, 91405 Orsay, France*

We study the translocation of a polymer chain through a nanopore where the chain length fluctuates stochastically due to the polymerization-depolymerization processes at the chain ends. We map this process to an equivalent representation where the pore performs a stochastic random-walk-like process on a line in the presence of two diffusing sinks on either side of it with diffusion constants D_1 and D_3 respectively. The translocation process terminates when the pore hits either of the two outer diffusing sinks. In the case where the pore motion itself is diffusive with diffusion constant D_2, we compute exactly the splitting probability that the pore hits the left (right) sink before hitting the right (left) sink. We show that the splitting probability in the presence of mobile sinks is rather nontrivial compared to the classical case of immobile sinks (the latter corresponds to the case when the chain length is fixed). Furthermore, we also compute exactly the probability distribution of the translocation time and that of the chain length at the completion time of the translocation. We show that both distributions have power law tails with exponents that depend continuously on the diffusion constants D_1, D_2 and D_3. We validate our analytical predictions via numerical simulations. We then present numerical results for the case when the pore performs a fractional Brownian motion with Hurst exponent $0 < H < 1$, while the sinks are still diffusive.

I. INTRODUCTION: TRANSLOCATION OF A POLYMER CHAIN THROUGH A PORE

The process by which a polymer chain passes through a narrow pore on a wall/membrane from one side to the other is known as the translocation process. Understanding this process is important in many physical, chemical and biological systems, and it has therefore been studied extensively over the past decades, leading to numerous applications[1–7]. In Fig. 1 (a), we show a schematic picture of this process for a polymer chain consisting of N monomers. The number of monomers, $s(t)$, to the right of the pore at time t, usually referred to as the translocation coordinate, is a key quantity for understanding the translocation process [5–7]. As a monomer passes through the pore to its right (left), the translocation coordinate $s(t)$ increases (decreases) by 1. Thus the translocation coordinate $s(t)$ undergoes a random-walk-like stochastic process [6, 8–10, 19]. The translocation process becomes complete when $s(t)$ either hits N or 0 for the first time. In the former case when $s(t)$ hits N before hitting 0, the chain translocates successfully from the left to the right of the pore. In contrast, if $s(t)$ hits 0 before hitting N, then the chain translocates from the right to the left of the pore. An alternative, but completely equivalent, description is to consider the pore itself as performing a stochastic hopping process on a fixed one-dimensional lattice whose sites are labelled $i = 0, 1, 2, \ldots, N, N + 1 = L$, see Fig. 1 (a). The two sites 0 and L at the two ends act like sinks. Whenever the 'stochastic' pore reaches either 0 or L, the process stops. If it reaches 0 first, this means that the number of monomers $s(t)$ to the right of the pore hits N and the translocation occurs from the left to the right of the pore. In contrast, if the stochastic pore reaches $L = N+1$ first, then the number of monomers to its right is 0 indicating translocation from the right to the left of the pore. We will refer to this alternative picture as representation (b) in the rest of the paper. We will see later that this representation (b) of the translocation process is convenient for the problem addressed in this paper.

Several studies have shown that the actual stochastic motion of the translocation coordinate $s(t)$, or equivalently that of the motion of the pore in representation (b) mentioned above, can be very complex as it depends on various factors such as the pore size, the solvent concentration, the excluded volume effect etc. [6, 8, 10, 19]. For large N, one can make a further approximation by replacing the lattice by a continuous interval over $[0, L]$ and assuming the translocation coordinate $s(t)$ is a continuous stochastic process in time.

Although the actual stochastic dynamics of the pore may be rather complicated in reality, it has been useful to study some generic properties of the translocation process via modeling it by some well-known stochastic process, such as the fractional Brownian motion (fBM) with Hurst exponent $0 < H < 1$ [19]. An fBM is a Gaussian process with zero mean and a correlator [11]

$$\langle s(t_1)s(t_2)\rangle = D\,\left[t_1^{2H} + t_2^{2H} - |t_1 - t_2|^{2H}\right]\,, \qquad (1)$$

where D is a non-negative constant. Note that for general $0 < H < 1$, the fBM is a non-Markovian process, except for $H = 1/2$, where it reduces the ordinary Brownian motion which is a Markov process [12, 13]. In this paper, we will first focus on ordinary Brownian motion ($H = 1/2$) for which several results can be derived analytically and then present some numerical results for other values of

* a.hartmann@uni-oldenburg.de
† satyanarayan.majumdar@cnrs.fr
‡ alberto.rosso74@gmail.com

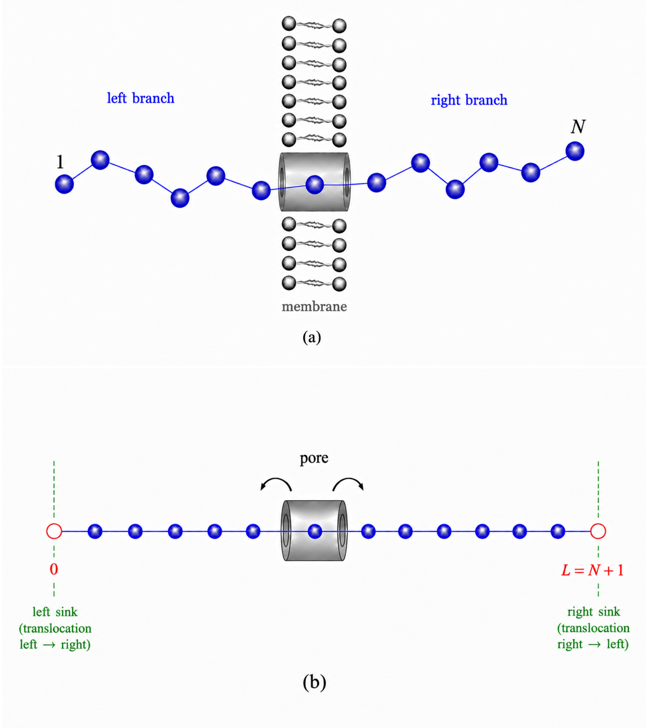

FIG. 1. (a) A schematic picture of a polymer chain, consisting of N monomers, translocating through a pore. The translocation process ends when the number of monomers to the right of the pore becomes either N (the chain then successfully translocates from left to right) or 0 (the chain translocates from right to left). (b) An alternative equivalent representation where the pore itself performs a stochastic nearest neighbour hopping on a lattice with $L = N + 1$ sites (labelled as $0, 1, 2, \ldots, L = N + 1$), and the process ends when the pore hits either the site 0 (translocation from left to right of the pore) or the site L (translocation from right to left of the pore). The two sites 0 and L (marked by dashed vertical lines) represent two sink sites for the 'moving' pore.

H. In representation (b) and in the continuum, the case $H = 1/2$ corresponds to the pore performing a Brownian motion with diffusion constant D in an interval $x \in [0, L]$ with two absorbing walls at $x = 0$ and $x = L$, see Fig. 2. The location of the pore at time t is denoted by $z_1(t)$ and hence, in this picture, the translocation coordinate is simply $s(t) = z_2(t) = L - z_1(t)$, as shown in Fig. 2. The pore starts from the initial location y_1, i.e., the initial value of the translocation coordinate is $y_2 = L - y_1$. The process stops when the Brownian pore hits either the wall at 0 (indicating translocation of the polymer chain from the left to the right of the pore) or the wall at L (translocation from right to left).

One can then study various observables associated with the actual translocation process within this simplified Brownian motion picture, where analytical results can be obtained. For example, one natural question is: what is the probability that the polymer chain will translocate from the left to the right of the pore? In the Brownian motion picture of representation (b), this is equivalent to asking the probability that the Brownian walker in Fig. 2, starting initially at y_1, will hit the left wall at 0 first before hitting the right wall at L. This is the classical 'splitting' probability (or sometimes called 'hitting' probability in the probability literature) [15, 16] of a Brownian motion starting at $y_1 = L - y_2$. In the context of the translocation process, y_2 is the initial value of the translocation coordinate $z_2(t = 0)$. Expressing everything in terms of the initial translocation coordinate y_2, for the walker, starting at $y_1 = L - y_2$, let

$$\begin{aligned} p_{\text{left}}(y_2|L) &= \text{Prob[walker hits the left wall first]} \\ p_{\text{right}}(y_2|L) &= \text{Prob[walker hits the right wall first]} \end{aligned} \tag{2}$$

Essentially, the net probability flux out of the box $[0, L]$ gets split between the left and the right with these probabilities, leading to the name splitting probabilities. Evidently, $p_{\text{left}}(y_2|L) + p_{\text{right}}(y_2|L) = 1$. The exact expressions for these splitting probabilities are incredibly simple [15, 16]

$$p_{\text{left}}(y_2|L) = \frac{y_2}{L} \quad \text{and} \quad p_{\text{right}}(y_2|L) = 1 - \frac{y_2}{L}\,. \tag{3}$$

Interestingly, the splitting probabilities are independent of the diffusion constant D of the Brownian motion. A simple derivation of this classical result using the backward Fokker-Planck equation is reproduced in Section II for the sake of completeness, as well as to illustrate the backward Fokker-Planck method. Splitting probability for several non-Brownian processes in one dimension has been computed exactly. This includes Lévy flights [17, 18], several anomalous subdiffusive processes [20], Brownian particle in the presence of an external potential [20], symmetric jump processes [21], active run-and-tumble particle in one dimension [22–24] etc. For a recent application of splitting probability of N Brownian motions subjected to simultaneous stochastic resetting triggered by the crossing of a threshold by any one of the walkers, see Ref. [25].

In this paper, we introduce a generalised model of Brownian translocation process where the chain length N of the polymer is not fixed, but fluctuates in time. For a polymer in a solvent, often the chain length decreases through depolymerization whereby a single monomer from either of the two edges can detach from the polymer with some rates [26–29]. Conversely, polymerization may also occur, whereby a new monomer can attach at either end of the chain with certain rates. For simplicity, we assume that at each end, the rates of polymerization and depolymerization are equal, but these rates can be different at the two ends. We denote these rates by λ_l (for the left end) and λ_r (for the right end), see Fig. 3 for a schematic representation. In the random walk representation (b), this means that the absorbing walls at 0 and L are not fixed in time, but their locations also diffuse, in addition to the Brownian motion of the pore in the middle. Since the left end polymerizes and depolymerizes with the same rate λ_l, in the representation (b) and

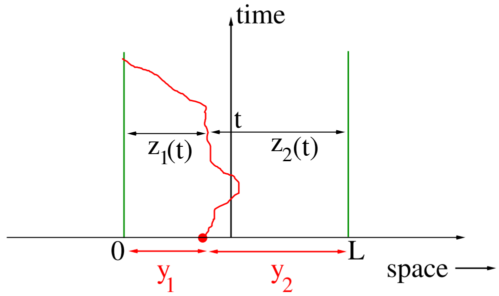

FIG. 2. A schematic trajectory of a single Brownian particle (shown by red solid line) diffusing in a box $[0, L]$, starting initially at $0 \leq y_1 \leq L$. The process stops when the walker hits either of the two boundaries at 0 or at L. In the displayed configuration, the walker hits the left boundary at 0 before hitting the right boundary.

in the continuum Brownian picture, this corresponds to the case where the left wall, initially located at 0, diffuses with a certain diffusion constant D_1 proportional to λ_l. Similarly, the right wall, initially located at L, also diffuses, but with a different diffusion constant D_3 proportional to λ_r. We also assume that the central Brownian pore, sandwiched between the two diffusing walls, itself diffuses with a diffusion constant D_2. Thus this translocation process for a polymer chain with fluctuating size, via polymerization/depolymerzation at the edges, then maps directly onto a model of three 'vicious' Brownian walkers on a line with diffusion constants $\{D_1, D_2, D_3\}$ and starting from initial separations y_1 (between the first and the second walker) and $y_2 = L - y_1$ (between the 2nd and the 3rd walker), see Fig. 3.

These walkers are called 'vicious' because the process terminates whenever any two of them meet meet. The vicious walker problem with M walkers was introduced by Karlin and McGregor in the probability literature [30] and by de Gennes [31] in the physics literarture, although the name 'vicious' was given by M. E. Fisher in the context of the dynamics of domain walls in commensurate-incommensurate system [32], Since then, the vicious walker problem has been studied extensively, both in the physics and in the mathematics literature [33–49]. The general M particle problem has mostly been studied in the case when all the diffusion constants are identical. In that case, conditioned on the process being alive up to time t (i.e., none of the M walkers meet another member up to t), the joint distribution of the positions of the walkers at time t, rescaled by $\sqrt{t}$, happens to be identical to the joint distribution of M eigenvalues of a real symmetric $(M \times M)$ Gaussian matrix (the so called Gaussian Orthogonal Ensemble) [36, 40, 41]. However, for different diffusion constants, the general M-particle problem is hard to solve. For $M = 3$ and with different diffusions constants $\{D_1, D_2, D_3\}$ which is the case of interest here, it turns out that several observables can be computed exactly, via a mapping to a diffusion process in a wedge in two dimensions [50–52]. This includes, in particular, the survival probability or the persistence of the process up to time t [16, 53]. However, we are interested here in the probability of translocation, i.e., the splitting probabilities $p_{\rm left}(y_2|L)$ and $p_{\rm right}(y_2|L) = 1 - p_{\rm left}(y_2|L)$ as defined in (2), but now for the case where the walls are Brownian walkers initially seperated at distance L.

To the best of our knowledge, the splitting probabilities for three Brownian walkers with different diffusion constants $\{D_1, D_2, D_3\}$ have not been studied before. In this paper, we present an exact solution of these splitting probabilities in Section III B (see Eqs. (30)).

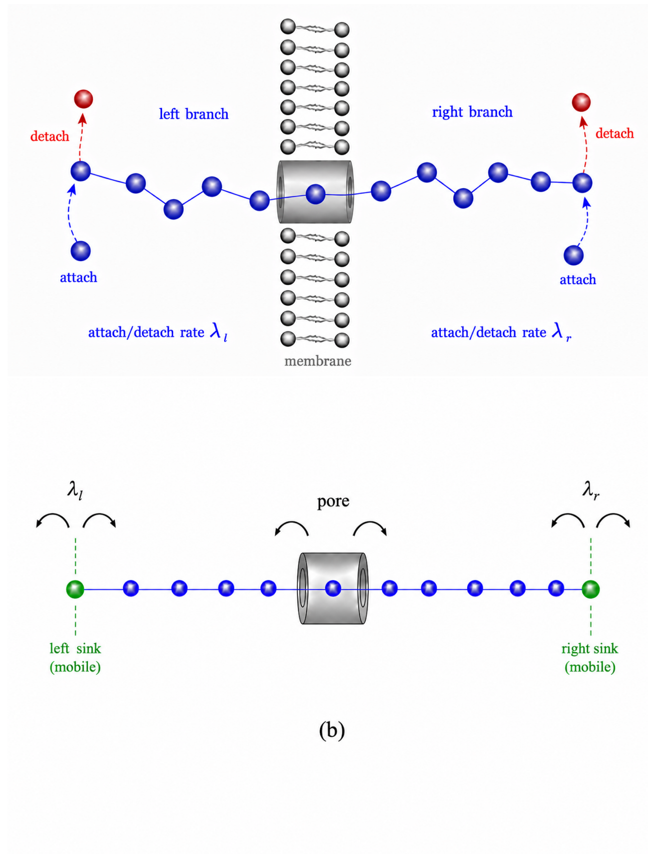

FIG. 3. (a) A schematic picture of a polymer chain translocating through a pore. The monomer located at the left end (shown by a red filled circle) can detach or attach with rate λ_l. Similarly the monomer located at the right edge (also shown by a red filled circle) can detach or attach with rate λ_r. (b) An alternative equivalent representation where the pore itself performs a stochastic nearest neighbour hopping on a lattice. Also, the two boundaries of the cluster representing the end monomers also perform 'random walk' like hopping to the left and to the right. The two sites at the end (now also moving stochastically) act like sinks. The translocation process ends when the central walker hits either the left or the right sink.

In this translocation process of a polymer chain with fluctuating size, there are additional observables of interest which are completely trivial in the fixed chain problem. For example, it is natural to ask: what is the distribution of the length of the polymer chain when it finishes the translocation process? In the case of fixed chain length, the length of the polymer chain at the time of the completion of the translocation process is trivially N. However, this distribution turns out to be nontrivial in the case of fluctuating chain size, as we show in this paper. More generally, one can ask what is the joint probability distribution $P^{\rm left}(t,z)$ that the translocation process (say from the left of the pore to its right) completes at time t and that the length of the chain at the time of the the completion is equal to z. In this paper, for the Brownian version of the translocation process, we compute this joint distribution $P^{\rm left}(t,z)$ exactly in Section IV (see Eqs. (61) and (62)). By integrating over z or over t, we then compute the marginal distribution of the time of completion, as well as the marginal distribution of the size of the polymer chain at the time of the completion of translocation. We show that the marginal distribution of the translocation time t_ℓ has a power-law decay for large t

$$P_{t_\ell}^{\rm left}(t) = \int_0^\infty P^{\rm left}(t,z)\, dz \approx \frac{C_1}{t^\kappa} \tag{4}$$

where the amplitude C_1 is a constant that depends on the initial separations and the exponent κ is given by

$$\kappa = 1 + \frac{\pi}{2\,\cos^{-1}\left(\frac{D_2}{\sqrt{(D_1+D_2)(D_2+D_3)}}\right)}\,. \tag{5}$$

Thus this exponent depends continuously on the three diffusion constants D_1, D_2 and D_3. Similarly, we show (see Section IV) that the marginal size distribution denoted by $P_z^{\rm left}(z)$ decays as a power law for large z

$$P_z^{\rm left}(z) = \int_0^\infty P^{\rm left}(t,z)\, dt \approx \frac{C_2}{z^\beta} \quad \text{as} \quad z\to\infty\,, \tag{6}$$

where C_2 is a constant (function of the initial separations) and the exponent β also depends continuously on the diffusion constants $\{D_1, D_2, D_3\}$. The exact expression for the exponent β reads

$$\beta = 1 + \frac{\pi}{\cos^{-1}\left(\frac{D_2}{\sqrt{(D_1+D_2)(D_2+D_3)}}\right)}\,. \tag{7}$$

These power-law decays of the two marginal distributions in Eqs. (4) and (6) are two main exact results of this paper. We also perform extensive numerical simulations to verify our analytical predictions for the splitting probabilities, the joint distribution $P^{\rm left}(t,z)$ and the result in Eqs. (6)-(7). We find excellent agreement between the theory and the simulations. We also present numerical results for the splitting probabilities and the marginal distributions of the translocation time t_ℓ and the chain length z at the completion time of the translocation for the case when the central particle performs an fBM with Hurst exponent $H \neq 1/2$, while the left and the right particles (the sink sites) perform ordinary Brownian motions.

The rest of the paper is organized as follows. In Section II, we first present an illustration of the backward Fokker-Planck method to derive the well-known result for the splitting probabilities of a Brownian motion in a fixed interval $[0,L]$. In Section III, we compute the splitting probability for a Brownian walker with diffusion constant D_2 and surrounded by two sinks performing independent Brownian motions with diffusion constants D_1 and D_3. We first present the numerical approach in Section III A and then in Section III B we present the exact analytical results. In Section IV, we compute exactly, for the three Brownian walkers model, the joint distribution of the hitting time of the central particle to its left neighbour (before the right neighbour) and the separation from the right neighbour at the time of hitting the left neighbour. In Section V, we present numerical results for the case when the central particle performs an fBM with Hurst exponent $H \neq 1/2$, while the two outer particles perform ordinary diffusions. Finally, we conclude with a summary and outlook in Section VI.

II. SPLITTING PROBABILITY FOR A BROWNIAN WALKER BETWEEN TWO FIXED WALLS

We first recall the well-known results for the splitting probability of a single Brownian walker diffusing inside an interval $[0,L]$ of length L. Here the walls/boundaries at $x=0$ and $x=L$ are fixed and do not change with time. The position $x(t)$ of the walker inside the interval evolves by the Langevin equation

$$\frac{dx}{dt} = \sqrt{2D}\,\eta(t)\,, \tag{8}$$

where D is the diffusion constant and $\eta(t)$ is a zero mean Gaussian white noise with correlator $\langle \eta(t)\eta(t')\rangle = \delta(t-t')$. The walker starts from the initial position $0 \le x(0) = y_1 \le L$ and the process stops when the walker hits either the left boundary at 0 or the right boundary at L. Let $y_2 = L - y_1$ denote its initial distance from the right wall at L (see Fig. 2). Let $z_1(t)$ and $z_2(t)$ denote the distances of the walker from the two walls at time t before it hits either of the walls (see Fig. 2). In the context of the translocation process discussed in the introduction, the separation $z_2(t)$ is precisely the translocation coordinate of the underlying polymer chain. Hence, y_2 is the initial value of the translocation coordinate.

When considering the splitting probabilities $p_{\rm left}(y_2|L)$ and $p_{\rm right}(y_2|L) = 1 - p_{\rm left}(y_2|L)$ as defined in (2), it is a classical result in probability theory that $p_{\rm left}(y_2|L)$ is given by the simple linear formula [15, 16] as shown in (3). Note that the splitting probability is independent of the diffusion constant D of the walker.

Equation (3) can be derived straightforwardly using the backward Fokker–Planck approach (for different applications of the backward method, see Refs. [53, 54]). Within this approach, it is easier to consider the dependency of the splitting on the initial position y_1, i.e., one monitors how the splitting probability $p_{\rm left}(y_1) \equiv p_{\rm left}(y_2 = L - y_1|L)$ changes as one varies the initial position y_1. Here, we do not need to keep track of the distance $z_1(t) = L - z_2(t)$ of the walker as a function of time t. Instead, we integrate over the entire history of the process and treat only the initial position y_1 of the walker as the relevant variable. Starting from y_1, during the first interval Δt, the walker moves to a new position $y_1 + \sqrt{2D}\eta(0)\,\Delta t$ after which it continues to diffuse from this new position. Here, $\eta(0)$ refers to the first kick (noise). Consequently

$$p_{\rm left}(y_1) = \langle p_{\rm left}(y_1 + \sqrt{2D}\eta(0)\,\Delta t\,)\rangle\,, \tag{9}$$

where $\langle\rangle$ refers to the average over the initial noise $\eta(0)$. Expanding in a Taylor series for small Δt up to the second order and using the properties of the white noise, namely $\langle\eta(0)\rangle = 0$ and $\langle\eta^2(0)\rangle = \frac{1}{\Delta t}$ (which follows from the delta correlator of the noise), one obtains from Eq. (9) an ordinary differential equation

$$D\,\frac{d^2 p_{\rm left}(y_1)}{dy_1^2} = 0\,. \tag{10}$$

This equation holds in $y_1 \in [0, L]$ with the boundary conditions: (i) $p_{\rm left}(y_1 = 0) = 1$ and (ii) $p_{\rm left}(y_1 = L) = 0$. The boundary condition (i) simply follows from the fact that if the walker starts at the left boundary, it will immediately exit through the left boundary and hence the probability of this event is 1. Similarly, (ii) follows from the fact that if the walker starts at the right boundary, the probability that it will hit the left boundary before hitting the right boundary is exactly zero. The solution to this differential equation satisfying the two boundary conditions is precisely given by

$$\begin{aligned} p_{\rm left}(y_1) &= 1 - \frac{y_1}{L}, \quad \text{and consequently} \\ p_{\rm right}(y_1) &= 1 - p_{\rm left} y_1 = \frac{y_1}{L}\,. \end{aligned} \tag{11}$$

It is also clear from Eq. (10) that the diffusion constant D just drops out of the solution.

In the context of the translocation process discussed in the introduction, it is useful to express these results in terms of the initial value of the translocation coordinate $y_2 = L - y_1$, which then leads to (3).

III. SPLITTING PROBABILITY FOR A BROWNIAN WALKER BETWEEN TWO DIFFUSING WALLS

We next consider a generalized model in one dimension where a single Brownian walker diffuses in the region sandwiched between between two walls as above, except that the walls themselves diffuse in time. In this section we introduce the model formally. Thus, we now consider three Brownian walkers on a line whose positions $x_i(t)$ ($i = 1, 2, 3$) evolve via independent Langevin equations

$$\frac{dx_i}{dt} = \sqrt{2D_i}\,\eta_i(t)\,, \tag{12}$$

where D_i's are the respective diffusion constants and $\eta_i(t)$'s are zero mean Gaussian white noises with correlator

$$\langle\eta_i(t)\eta_j(t')\rangle = \delta_{i,j}\,\delta(t - t')\,. \tag{13}$$

The walkers start from ordered initial positions satisfying $x_1(0) < x_2(0) < x_3(0)$. The process stops when the middle walker hits either of the moving boundaries on the left or the right (see Fig. 4). Let $y_1 = x_2(0) - x_1(0)$ and $y_2 = x_3(0) - x_2(0)$ denote the initial gaps, as in Section II for the case of fixed walls. Let us denote the the splitting probabilities by $p_{\rm left}(y_1, y_2)$ and $p_{\rm right}(y_1, y_2)$ for first hitting the left and right walls, respectively. This is equivalent to the definition Eq. (2), but now depends explicitly on two distances, which we will use below for the analytical calculation. Evidently, $p_{\rm left}(y_1, y_2) + p_{\rm right}(y_1, y_2) = 1$. Note that when $D_1 = D_3 = 0$, this problem reduces precisely to the fixed-wall problem with $D = D_2$ as studied in Section II. Below, we first describe the numerical approach in Section III A and then present the exact analytical result in Section III B.

A. Numerical approach to compute the splitting probability

Since we compare our analytical results with numerical simulations [55] throughout the paper, we first briefly describe the simulation procedure. The basic idea is to simulate Brownian motions for the walkers $x_i(t)$, $i = 1, 2, 3$. For simplicity, let us first consider Eq. (12) with the initial condition $x_i(0) = 0$. Then the position distributions at time t are given by

$$p_t(x_i) = \frac{1}{\sqrt{4\pi D_i t}}\exp\left(-\frac{x_i^2}{4D_i t}\right) \tag{14}$$

i.e., a Gaussian with zero mean and standard deviation $\sqrt{2D_i t}$. If the walkers start at non-zero initial positions $x_i(0)$, the probability distributions are correspondingly shifted.

This solution is true also for small time intervals of size Δt, which can be interpreted as the relative movement, i.e., a step, of a walker within the small time interval, as utilized within a numerical simulation. Summing up several steps leads to the walk. This is described by a discretised version of the Langevin equation for a time series $x(0)$, $x(\Delta t)$, $x(2\,\Delta t), \ldots$ at discretised times $t = k\Delta t$ ($k = 0, 1, 2, \ldots k_{\rm max}$) until the final time $t_{\rm max} = k_{\rm max}\Delta t$. and reads

$$x_i((k+1)\Delta t) = x_i(k\Delta t) + \sqrt{2D_i\Delta t}\,\xi_i(k)\,, \tag{15}$$

with indendependent and identically distributed (iid) random numbers $\xi_i(k)$ which are Gaussian distributed with zero mean and variance one. Note that these equations do not carry any discretisation error at the measured times $t = k\Delta t$.

Since one main interest of this study is first-passage or first-splitting properties, this will lead to approximations: between the measured positions $x_i(k\Delta t)$ the behavior is not known precisely, except that the paths will not be "far away" from the measured positions, respectively. For the average behavior, if Δt is chosen small enough, this will not matter much, as we see for our results. We have used mostly $\Delta t = 10^{-5}$ in this work and did tests for $\Delta t = 10^{-4}$ which did not significantly change the results. Thus, for those simulations, where the final time and the number of independent runs are large, we used $\Delta t = 10^{-4}$. Note that a more efficient and accurate but more complex algorithm with adaptive time steps can certainly be devised. This has already been done for the first-passage time properties of a single Brownian walker with a single non-moving target [56]. The main idea of that algorithm is to adaptively splitting those time intervals where with large-enough probability a hitting event occurs. Such an algorithm would, in particular, be useful if one is interested in short time properties. Here, as mentioned, we simply choose Δt small enough to measure our quantities of interest. As we will see below, we observe very good agreement between numerical and analytical results, which shows that the time steps we have chosen are small enough.

One main quantity of interest is the left-hitting probability $p_{\text{left}}(y_2|L)$ which depends on the initial distance $y_2 = x_3(0) - x_2(0) = L - x_2(0)$ of the middle to the right walker, i.e., on $x_2(0)$. One could perform simulations for many values of $y_2 \in [0, L]$ but that would be tedious. Instead, we generate just three random walks and check a set $0 < l_1 < l_2 < \ldots < l_N < L$ of N starting positions for the middle walker $x_2(0)$. Here we consider equally spaced position $l_n = n\Delta x$ for suitable small spatial resolution Δx, here $\Delta x = L/(N+1)$, typically we use $N = 50$. Now, one *run* consist of generating three time series $\{x_i(t)\}$ with $x_1(0) = x_2(0) = 0$ and $x_3(0) = L$. The output of the analysis consist of two vectors $\tilde{p}_{\text{left}}(l_n) \in \{0, 1\}$ and $\tilde{p}_{\text{right}}(l_n) \in \{0, 1\}$ $(n = 1, \ldots, N)$ which tell whether for given set of three time series, the middle walker starting at the position $y_2 = l_n$, leads to hitting the left or right moving wall first, respectively. These checks can be done rather quickly, because for each time t one has to check only an interval $I = [l_{\text{left}}, l_{\text{right}}]$ of starting positions $x_2 \in I$, where I is always chosen such that neither hitting the left nor the right boundary has been observed until the current time t. Hence, initially, ate time $t = 0$, one has $I = [l_1, l_N]$. With increasing time t, more and more hitting events for some starting positions of x_2 are observed and the interval $[l_{\text{left}}, l_{\text{right}}]$ shrinks. The check is finished when I is empty, i.e., for all considered values of $x_2(0)$ a hit of the middle walker with a boundary has been observed. This process achieved is by the following algorithm:

algorithm check_boundary($t_{\max}$, $\{x_i(t)\}$, $\{l_i\}$)
begin
  initialize all $\tilde{p}_{\text{left}}(l_n) = \tilde{p}_{\text{right}}(l_n) = 0$;
  set $t = 0$; $l_{\text{left}} = l_1$, $l_{\text{right}} = l_N$
  while ($t < t_{\max}$ AND $l_{\text{left}} < l_{\text{right}}$)
    for $l = l_{\text{left}} \ldots l_{\text{right}}$ (iterate start)
    begin
      if ($l + x_2(t) < x_1(t)$) **then** (hit left)
        set $\tilde{p}_{\text{left}}(l) = 1$; $l_{\text{left}} = l + \Delta x$;
      if ($l + x_2(t) > x_3(t)$) **then** (hit right)
      begin
        set all $\tilde{p}_{\text{left}}(l) = 1 \ldots \tilde{p}_{\text{left}}(l_{\text{right}}) = 1$;
        $l_{\text{right}} = l - \Delta x$;
      end
      $t = t + \Delta t$;
    end
  return ($\{\tilde{p}_{\text{left}}(l_n), \tilde{p}_{\text{right}}(l_n)\}$);
end

When averaging over a certain number of runs, we usually did 10^4, the averages of $\tilde{p}_{\text{left}}(l_n)$ and $\tilde{p}_{\text{left}}(l_n)$ will result for the considered values $y_2 = L - l_n$ $(n = 1, \ldots, N)$ in estimates for $p_{\text{left}}(y_2|L)$ and $p_{\text{right}}(y_2|L)$. Note that due to the discretisation in time, it might happen that for a run and a given starting position l_n one observes hits both with the left and right boundary at the same time, within the discretisation accuracy. For a test with $\Delta t = 10^{-5}$ it happened never in 10^4 runs, but for $\Delta t = 10^{-4}$, which we used sometimes, it happened just 16 times, combined for all possible starting positions together. This has no visible effect on the results.

As mentioned earlier, we considered the movements only until a maximum time $t_{\max}$. This leads to very few cases for some values of the initial positions $x_2(0) = l_n$ for which a small fraction of trajectories remain undecided, as visible from $\tilde{p}_{\text{left}}(l_n) = \tilde{p}_{\text{left}}(l_n) = 0$ after the algorithm has finished. For our choice $L = 1$ and $t_{\max} = 10$ this happens for a fraction of at most 10^{-3} of the runs, which is not visible in the $p_{\text{left}}(y_2|L)$ plots.

We also measure numerically the joint distribution of times t of the middle walker hitting the left boundary and the corresponding distances $z = x_3(t) - x_2(t)$ from the right boundary. Here, we have restricted ourselves to the middle starting position $x_2(0) = L/2$ of the middle walker to save the amount of stored data.

B. Exact result for the splitting probability

We first introduce the gap variables $z_1(t) = x_2(t) - x_1(t)$ and $z_2(t) = x_3(t) - x_2(t)$. Using Eq. (12) it is easy to see that they evolve via the pair of Langevin equations

$$\frac{dz_1}{dt} = \sqrt{2D_1}\,\eta_1(t) - \sqrt{2D_2}\,\eta_2(t) = \xi_1(t) \qquad (16)$$

$$\frac{dz_2}{dt} = \sqrt{2D_3}\,\eta_3(t) - \sqrt{2D_2}\,\eta_2(t) = \xi_2(t) \qquad (17)$$

where $\xi_{1,2}(t)$ are again zero-mean Gaussian white noises, but they are correlated since they share the same noise $\eta_2(t)$. The correlators of these noises are given by

$$\begin{aligned} \langle \xi_1(t)\xi_1(t')\rangle &= 2(D_1+D_2)\,\delta(t-t') \\ \langle \xi_2(t)\xi_2(t')\rangle &= 2(D_2+D_3)\,\delta(t-t') \\ \langle \xi_1(t)\xi_2(t')\rangle &= -2D_2\delta(t-t')\,. \end{aligned} \tag{18}$$

Thus the noises $\xi_1(t)$ and $\xi_2(t)$ are anti-correlated. This anticorrelation is expected because if the central particle moves to the left (or right), the gap $z_1(t)$ decreases (increases) while the gap $z_2(t)$ increases (decreases), leading to the anti-correlation. The 'two-dimensional' gap process $(z_1(t), z_2(t))$ starts from the initial condition $(z_1(0) = y_1, z_2(0) = y_2)$. Our goal is to compute the splitting probability $p_{\rm left}(y_1, y_2)$, i.e., the probability of the event when $z_1(t)$ hits zero before $z_2(t)$ does so.

To compute this splitting probability, we again use the backward Fokker-Planck approach using the Langevin equations (16) and (17). As in the previous subsection, we now evolve the two-dimensional process $(z_1(t), z_2(t))$ from its initial value (y_1, y_2) in the first step of duration Δt. In this first step, the two-dimensional process moves to $(y_1+\xi_1(0)\,\Delta t, y_2+\xi_2(0)\,\Delta t)$ and the process diffuses subsequently starting from this new position. Here $(\xi_1(0), \xi_2(0))$ refers to the first kick or noise to the process. Hence it follows that

$$p_{\rm left}(y_1, y_2) = \langle p_{\rm left}(y_1+\xi_1(0)\,\Delta t, y_2+\xi_2(0)\,\Delta t)\rangle\,, \tag{19}$$

where $\langle \dots \rangle$ refers to the average over the initial noises $(\xi_1(0), \xi_2(0))$. Expanding in Taylor series for small Δt up to the second order and using the properties of the noise correlators in Eq. (19), one gets a two-dimensional partial differential equation in the (y_1, y_2) plane, or more precisely in the $(y_1 \geq 0, y_2 \geq 0)$ quadrant

$$(D_1+D_2)\,\frac{\partial^2 p_{\rm left}}{\partial {y_1}^2} + (D_2+D_3)\,\frac{\partial^2 p_{\rm left}}{\partial {y_2}^2} - 2D_2\,\frac{\partial^2 p_{\rm left}}{\partial y_1 \partial y_2} = 0\,. \tag{20}$$

It satisfies the two boundary conditions: (i) $p_{\rm left}(y_1 = 0, y_2) = 1$ and (ii) $p_{\rm left}(y_1, y_2 = 0) = 0$. In case (i), if the process starts from $y_1 = 0$, then the probability that it hits the left boundary before the right boundary is surely 1. In contrast, in case (ii), it the initial value $y_2 = 0$, the central walker surely hits the right boundary before the left and hence $p_{\rm left}(y_1, y_2 = 0) = 0$.

To solve Eq. (20) it is convenient first to make a change of variables $(y_1, y_2) \to (w_1, w_2)$ to get rid of the off-diagonal term $-2\,D_2\,\frac{\partial^2 p_{\rm left}}{\partial y_1 \partial y_2}$ in Eq. (20) and reduce it to a standard isotropic Laplace's equation. The same change of variables was used before in the context of computing the distribution of the maximum displacement between the leader and the laggard in the 3-walkers problem [52]. This amounts to essentially diagonalize the (2×2) matrix with elements $[D_1+D_2, -D_2, -D_2, D_2+D_3]$. The change of variable that achieves this diagonalization can be written as

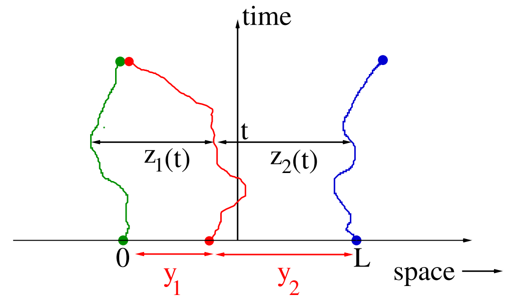

FIG. 4. A schematic trajectory of a single Brownian particle $x_2(t)$ (shown by the red solid line) diffusing between two moving walls: the left wall $x_1(t)$ starts at 0 (its trajectory shown by the green solid line) and the right wall $x_3(t)$ starts at L (with a blue trajectory). The initial gaps are denoted by $0 \leq y_1 \leq L$ and $0 \leq y_2 \leq L$, with $y_1 + y_2 = L$. The process stops when the middle walker hits either the left boundary or the right boundary. In the displayed configuration, the walker hits the left boundary before hitting the right boundary. We also denote the gaps between the positions of the walkers by $z_1(t) = x_2(t) - x_1(t)$ and $z_2(t) = x_3(t) - x_2(t)$ at time t before the process stops.

$$\begin{aligned} w_1 &= \frac{\sqrt{D_0}}{\sqrt{2-\gamma}}\left[\frac{y_1}{\sqrt{D_1+D_2}} + \frac{y_2}{\sqrt{D_2+D_3}}\right] \\ w_2 &= \frac{\sqrt{D_0}}{\sqrt{2+\gamma}}\left[-\frac{y_1}{\sqrt{D_1+D_2}} + \frac{y_2}{\sqrt{D_2+D_3}}\right] \end{aligned} \tag{21}$$

where we have defined

$$\gamma = \frac{2D_2}{\sqrt{(D_1+D_2)(D_2+D_3)}}\,. \tag{22}$$

In Eq. (21), we have included a constant D_0 in order that w_i's have the same dimensions (length) as the y_i's. One can choose any positive value of D_0 and we will see shortly that the splitting probability $p_{\rm left}(y_1, y_2)$ is independent of the actual value of D_0, as long as it is nonzero and positive. Under this change of variables, Eq. (20) simply reduces to the Laplace's equation in the (w_1, w_2) plane

$$D_0\left[\frac{\partial^2 p_{\rm left}}{\partial w_1^2} + \frac{\partial^2 p_{\rm left}}{\partial w_2^2}\right] = 0\,, \tag{23}$$

which shows immediately that D_0 drops out. The lines $y_1 = 0$ and $y_2 = 0$ in the (y_1, y_2) plane, under the change of variables (21), translate into a pair of straight lines $w_2 = \pm\tan(\alpha)\,w_1$ where

$$\alpha = \tan^{-1}\left(\sqrt{\frac{2-\gamma}{2+\gamma}}\right)\,. \tag{24}$$

Hence, the quadrant $(y_1 \geq 0, y_2 \geq 0)$ transforms into the wedge in the (w_1, w_2) plane bounded by the straight lines $w_2 = \pm\tan(\alpha)\,w_1$ (see Fig. 5). The wedge angle is $\alpha_W = 2\alpha$. Consequently, we need to solve the Laplace's equation (23) in this wedge in the (w_1, w_2) plane with boundary conditions: (i) $p_{\rm left}(w_1, w_2) = 1$ along $w_2 = \tan(\alpha)\,w_1$ and (ii) $p_{\rm left}(w_1, w_2) = 0$ along $w_2 = -\tan(\alpha)\,w_1$.

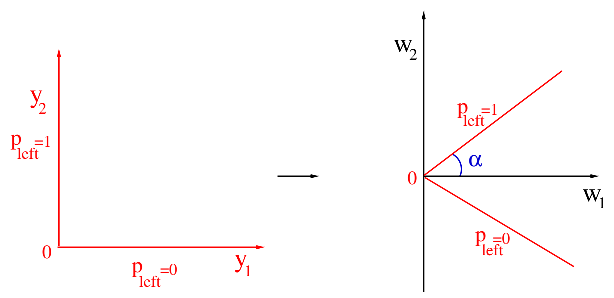

FIG. 5. Under the change of variables in Eq. (21), the quadrant $(y_1 \geq 0, y_2 \geq 0)$ in the (y_1, y_2) plane maps onto a wedge in the (w_1, w_2) plane, bounded by the two lines $w_2 = \pm\tan(\alpha)\,w_1$ with wedge angle $\alpha_W = 2\alpha$. The boundary conditions $p_{\rm left}(y_1 = 0, y_2) = 1$ and $p_{\rm left}(y_1, y_2 = 0)$ in the (y_1, y_2) plane accordingly translate into the boundary conditions on the two lines bounding the wedge in the (w_1, w_2) plane.

The wedge geometry naturally suggests that it would be easier to solve the Laplace's equation (23) in polar coordinates $(w_1, w_2) \to (r, \phi)$, where it reads

$$\frac{\partial^2 p_{\rm left}}{\partial_r^2} + \frac{1}{r}\frac{\partial p_{\rm left}}{\partial r} + \frac{1}{r^2}\frac{\partial^2 p_{\rm left}}{\partial \phi^2} = 0\,, \tag{25}$$

valid for $r \geq 0$ and $-\alpha \leq \phi \leq \alpha$ with boundary conditions: (i) $p_{\rm left}(r, \phi = \alpha) = 1$ and $p_{\rm left}(r, \phi = -\alpha) = 0$ for all $r \geq 0$. The fact that the boundary conditions must hold for any $r \geq 0$ indicates that the solution must be independent of r. In fact, assuming $p_{\rm left}(\phi)$ to be independent of r shows that it must satisfy

$$\frac{d^2 p_{\rm left}(\phi)}{d\phi^2} = 0\,, \tag{26}$$

whose general solution is $p_{\rm left}(\phi) = a_1 + b_1\,\phi$. The boundary conditions (i) and (ii) fixes the two unknown constants a_1 and b_1 and we obtain the full solution

$$p_{\rm left}(\phi) = \frac{1}{2}\left(1 + \frac{\phi}{\alpha}\right)\,, \tag{27}$$

where the angle α is given in Eq. (24). We note that the polar angle is given by

$$\phi = \tan^{-1}\left(\frac{w_2}{w_1}\right)\,. \tag{28}$$

Substituting (28) in Eq. (27) and transforming back to the original coordinates (y_1, y_2) via Eq. (21) we get our desired exact solution for the splitting probability

$$p_{\rm left}(y_1, y_2) = \frac{1}{2} + \frac{1}{2\,\tan^{-1}\left(\sqrt{\frac{2-\gamma}{2+\gamma}}\right)} \tan^{-1}\left[\sqrt{\frac{2-\gamma}{2+\gamma}}\,\frac{\left(-\frac{y_1}{\sqrt{D_1+D_2}} + \frac{y_2}{\sqrt{D_2+D_3}}\right)}{\left(\frac{y_1}{\sqrt{D_1+D_2}} + \frac{y_2}{\sqrt{D_2+D_3}}\right)}\right]\,, \tag{29}$$

where γ is defined in Eq. (22). Note that using $y_1 + y_2 = L$, we can eliminate y_1 in terms of y_2 in (29) and express $p_{\rm left}(y_2|L)$ only in terms of y_2 and L in a more compact form. It reads,

$$p_{\rm left}(y_2|L) = \frac{1}{2}\left[1 + \frac{1}{\tan^{-1}(a)}\,\tan^{-1}\left(a\,\frac{y_2(b+1) - L}{y_2(b-1) + L}\right)\right]\,, \tag{30}$$

for $0 \leq y_2 \leq L$, where the two constants a and b are given by

$$a = \sqrt{\frac{2-\gamma}{2+\gamma}} \quad \text{and} \quad b = \sqrt{\frac{D_1 + D_2}{D_2 + D_3}}\,. \tag{31}$$

Near the two limits $y_2 \to 0$ and $y_2 \to L$, the splitting probability has the asymptotic behaviors

$$p_{\rm left}(y_2|L) \approx \begin{cases} \frac{a\,b}{(1+a^2)\,\tan^{-1}(a)}\,\frac{y_2}{L} & \text{as} \quad y_2 \to 0 \\ 1 - \frac{a}{(1+a^2)b\tan^{-1}(a)}\,\frac{(L-y_2)}{L} & \text{as} \quad y_2 \to L\,. \end{cases}$$

Thus, unlike the fixed wall case where the splitting probability $p_{\rm left}(y_2|L)$ was a simple linear function in $y_2 \in [0, L]$, the exact result (30) for the moving walls case is nonlinear and has a richer structure.

As a useful consistency check of the exact result in (30), we note that for $D_1 = D_3 = 0$ (corresponding to fixed walls), we have $\gamma = 2$ from Eq. (22). Taking the $\gamma \to 2$ limit in Eq. (30) gives a linear curve

$$p_{\rm left}(y_2|L) = \frac{y_2}{L}\,, \quad 0 \leq y_2 \leq L\,. \tag{32}$$

We thus recover, as expected, the solution (3) for the fixed wall case. Another interesting special case corresponds to $D_1 = D_2 = D_3 = D$. In this case, we get $\gamma = 1$ from (22). Using $\tan^{-1}(1/\sqrt{3}) = \pi/6$, Eq. (30) gives the splitting probability

$$p_{\rm left}(y_1, y_2) = \frac{1}{2} + \frac{3}{\pi}\,\tan^{-1}\left(\frac{2\,y_2 - L}{\sqrt{3}\,L}\right)\,. \tag{33}$$

In Fig. 6, we compare our analytical prediction in Eq. (30) with numerical simulations for several choices of (D_1, D_2, D_3), using $t_{\rm max} = 10$, averaged over 10^4 independent runs, finding excellent agreement. For all results we have used the same diffusion $D_2 = 1$ for the middle walker. For fixed boundaries, i.e., $D_1 = D_3 = 0$, the behavior follows the straight line Eq. (3). The stronger the diffusion of the walks, i.e., the larger D_1 and D_2, the stronger are the deviations from the straight line.

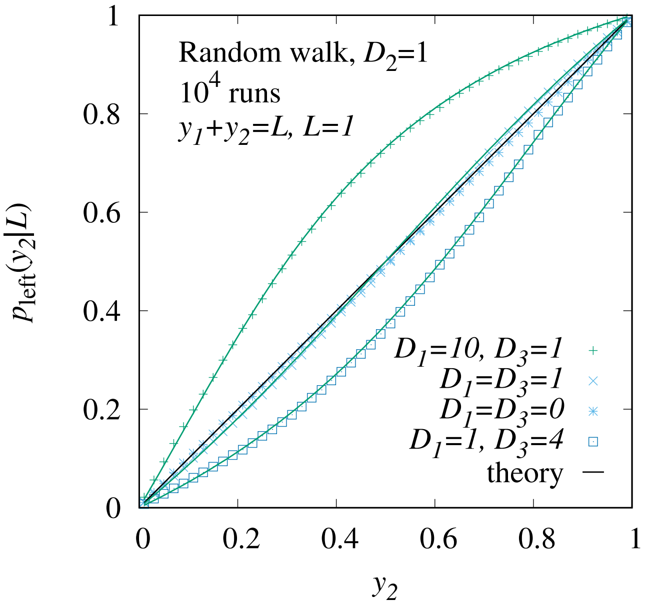

FIG. 6. Theoretical prediction for the splitting probability $p_{\rm left}(y_2|L)$ as a function of y_2 in Eq. (30), shown as lines in different colors, compared with numerical simulations, shown as symbols, for different choices of D_1 and D_3 (with $D_2 = 1$ and $L = 1$ fixed). One sees excellent agreement between the theory and simulations.

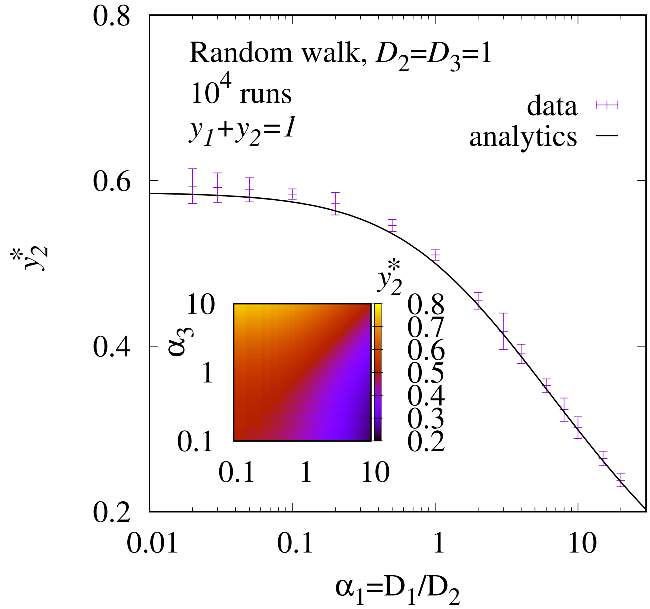

FIG. 7. Theoretical prediction for the halfpoint $y_2^*(\alpha_1)$ (where the left and right splitting probabilities are exactly equal) as a function of α_1 in (36) is shown by the solid black line. The numerical data points are shown by + symbols. In the inset, we show a heat map of y_2^* in (35) in the (α_1, α_3) plane (we have set $L = 1$).

Finally, we make an interesting observation. In the case of fixed walls ($D_1 = 0, D_2, D_3 = 0$), it is clear from (3) that exactly at the midpoint $y_2 = y_2^* = L/2$, the splitting probabilities $p_{\rm left} = p_{\rm right} = 1/2$. This just follows from symmetry. However, for moving walls with nonzero diffusion constants D_1 and D_3, there is no obvious symmetry, and consequently the splitting probabilities are generally different from $1/2$ at the midpoint, as visible in Fig. 6. It is then natural to ask for what value of $y_2 = y_2^*$, the left and right splitting probabilities are exactly equal to each other in the general case? Setting $p_{\rm left}(y_2^*|L) = 1/2$ in the exact result (30), it follows that this symmetrical point occurs at

$$y_2^* = \frac{L}{b+1}\,, \quad \text{and} \quad y_1^* = L - y_2^* = \frac{b\,L}{b+1}\,; \qquad (34)$$
$$\text{where } b = \sqrt{\frac{D_1+D_2}{D_2+D_3}}\,.$$

In terms of the ratios $\alpha_1 = D_1/D_2$ and $\alpha_3 = D_3/D_2$, the halfpoint y_2^* in (34) reads

$$\begin{aligned} y_2^* &= \frac{\sqrt{D_2+D_3}}{\sqrt{D_1+D_2}+\sqrt{D_2+D_3}}\,L \\ &= \frac{\sqrt{1+\alpha_3}}{\sqrt{1+\alpha_1}+\sqrt{1+\alpha_3}}\,L\,. \end{aligned} \qquad (35)$$

For $D_1 = D_3 = 0$, we clearly recover the fixed wall result $y_2^* = y_1^* = L/2$. We verify this analytical prediction via numerical simulation in Fig. 7, where, in the main figure, we have set $D_2 = D_3 = 1$ and $L = 1$. In this case $\alpha_3 = 1$ and $\alpha_1 = D_1$. From Eq. (35), setting $\alpha_3 = 1$, the halfpoint $y_2^*(\alpha_1)$ as a function of α_1 is given by

$$y_2^*(\alpha_1) = \frac{\sqrt{2}}{\sqrt{2}+\sqrt{1+\alpha_1}}\,. \qquad (36)$$

In the main curve of Fig. 7, we compare this theoretical prediction with numerical simulations, finding excellent agreement. The inset in Fig. 7 shows a heat map of y_2^* in Eq. (35) in the (α_1, α_3) plane.

IV. JOINT DISTRIBUTION OF THE HITTING TIME AND THE SEPARATION

In the previous section, we studied the splitting probabilities $p_{\rm left}(y_2|L)$ and $p_{\rm right}(y_2|L) = 1 - p_{\rm left}(y_2|L)$ as defined in Eq. (2). In this section, we study two other observables in this process. Conditioned on the event that the process terminates by hitting the left boundary, let t_ℓ denote the time at which this hapens (see Fig. 8). Also, at the hitting time of the left boundary t_ℓ, we denote by $z_2(t_\ell) = z$ the separation between the central particle and the right boundary (see Fig. 8). Clearly, both t_ℓ and $z_2(t_\ell) = z$ are random variables as they fluctuate from one realization to another. Moreover they are generally correlated. The main goal of this section is to compute the joint distribution of these two random variables, defined as

$$P^{\text{left}}(t,z)\,dt\,dz = \quad (37)$$

$$\text{Prob.}\,[t_\ell \in [t, t+dt] \,\text{and}\, z_2(t_\ell) \in [z, z+dz]]\,. \quad (38)$$

This conditional joint distribution is normalized to unity, i.e., $\int_0^\infty \int_0^\infty P^{\text{left}}(t,z)\,dt\,dz = 1$. From this normalized joint distribution, we can then derive the marginal distributions of the random variables t_ℓ and $z_2(t_\ell)$ by integrating out the other variable. We will denote these marginal distributions as follows

$$P_{t_\ell}^{\text{left}}(t) = \int_0^\infty P^{\text{left}}(t,z)\,dz\,, \quad (39)$$

$$P_z^{\text{left}}(z) = \int_0^\infty P^{\text{left}}(t,z)\,dt\,. \quad (40)$$

Of course, the joint distribution $P^{\text{left}}(t,z)$ also depends on the initial gaps y_1 and y_2, but we suppress this dependence in $P^{\text{left}}(t,z)$ for notational simplicity.

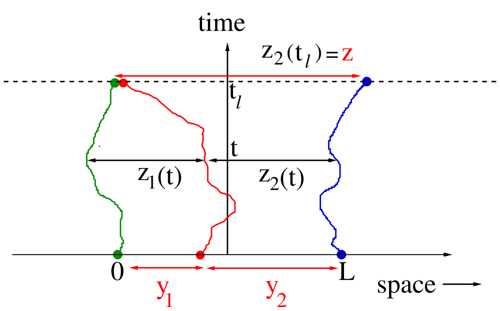

FIG. 8. A schematic trajectory of a single Brownian particle $x_2(t)$ (shown by the red solid line) diffusing between two diffusing walls: the left wall $x_1(t)$ starts at 0 (its trajectory shown by the green solid line) and the right wall $x_3(t)$ starts at L (with a blue trajectory). The initial gaps are denoted by $0 \le y_1 \le L$ and $0 \le y_2 \le L$, with $y_1 + y_2 = L$. We will consider the conditioned process where the process terminates by the central particle hitting the left boundary first. In this figure, we show a realization of the conditioned process where t_ℓ denotes the time of completion and $z_2(t_l) = z$ denotes the gap between the central particle and the right boundary at the time of completion. We also denote the gaps between the positions of the walkers by $z_1(t) = x_2(t) - x_1(t)$ and $z_2(t) = x_3(t) - x_2(t)$ at time t before the process stops.

For the computation of the splitting probabilities in the previous section, it was convenient to use the backward Fokker-Planck approach in Eq. (20) where the initial gaps y_1 and y_2 were treated as variables. This was possible because we were not interested there on the actual completion time at which the central particle hits either the left or the right boundary. However, if we want to compute the distributions of t_ℓ and $z_2(t_\ell)$, we need to keep track of the trajectories as time progresses. Hence, here we need to employ the forward Fokker-Planck approach where the separations $(z_1(t), z_2(t))$ at time t will be treated as variables. Let $P(z_1, z_2, t)$ denote the probability distribution of $(z_1(t), z_2(t))$ at time t (before the process terminates). Then, from the Langevin equations (16) and (17), one can derive the forward Fokker-Planck equation by increasing the time from t to $t+\Delta t$ and keeping track of how the distribution evolves. More precisely,

$$P(z_1, z_2, t+\Delta t) = \langle P(z_1 - \xi_1(t)\,\Delta t, z_2 - \xi_2(t)\,\Delta t, t)\rangle\,, \quad (41)$$

where $\langle\rangle$ denotes the average over the noises $(\xi_1(t), \xi_2(t))$ at time t. Note that in order to arrive at (z_1, z_2) at time $t+\Delta t$, the process must have been at $(z_1 - \xi_1(t)\Delta t, z_2 - \xi_2(t)\,\Delta(t))$ at time t and then reaches (z_1, z_2) by receiving the stochastic increments $(\xi_1(t), \xi_2(t))$ at time t. Finally, since these increments are stochastic, one must average over them as in Eq. (41). Expanding in Δt for small Δt up to $O((\Delta t)^2)$ and using the properties of noise correlators in Eq. (19), it is easy to show that $P(z_1, z_2, t)$ satisfies the forward Fokker-Planck equation

$$\frac{\partial P}{\partial t} = (D_1 + D_2)\,\frac{\partial^2 P}{\partial z_1^2} + (D_2 + D_3)\,\frac{\partial^2 P}{\partial z_2^2} - 2\,D_2\,\frac{\partial^2 P}{\partial z_1 \partial z_2}\,, \quad (42)$$

valid in the region $z_1 \ge 0$ and $z_2 \ge 0$, with the absorbing boundary conditions: (i) $P(z_1 = 0, z_2, t) = 0$ and (ii) $P(z_1, z_2 = 0, t) = 0$ and the initial condition

$$P(z_1, z_2, 0) = \delta(z_1 - y_1)\,\delta(z_2 - y_2)\,. \quad (43)$$

Note that if we integrate $P(z_1, z_2, t)$ over $z_1 \ge 0$ and $z_2 \ge 0$, it gives the survival probability

$$S(t) = \int_0^\infty \int_0^\infty P(z_1, z_2, t)\,dz_1\,dz_2\,, \quad (44)$$

that denotes the probability that the process is still alive at time t, i.e., the probability that the central particle does not hit either of the two boundaries up to time t. Integrating Eq. (42) over z_1 and z_2 and using the boundary conditions (i) and (ii) above, one finds

$$\begin{aligned} F(t) = -\frac{dS}{dt} &= (D_1 + D_2) \int_0^\infty dz_2\, \frac{\partial P}{\partial z_1}\Big|_{z_1=0} \\ &\quad + (D_2 + D_3) \int_0^\infty dz_1\, \frac{\partial P}{\partial z_2}\Big|_{z_2=0} \quad (45) \\ &= F_{\text{left}}(t) + F_{\text{right}}(t)\,. \end{aligned}$$

This equation admits a nice physical interpretation. The quantity $F(t) = -dS/dt$ on the left hand side (lhs) denotes the total probability flux leaving the system through the two boundaries at time t and hence it is exactly the first-passage probability density $F(t)$. Here $F(t)\,dt$ denotes the probability that the process completes exactly between $[t, t+dt]$ via the central particle hitting either the left or the right boundary. This total probability flux out of the system can be decomposed into two parts: (a) $F_{\text{left}}(t) = (D_1 + D_2)\int_0^\infty dz_2\, \frac{\partial P}{\partial z_1}\Big|_{z_1=0}$ denotes the probability current through the left boundary at time t and (b) $F_{\rm right}(t) = (D_2 + D_3) \int_0^\infty dz_1 \, \frac{\partial P}{\partial z_2}\Big|_{z_2=0}$ denotes the probability flux through the right boundary at time t. Note that the splitting probabilities, studied in the previous section by the backward Fokker-Planck method, can alternatively be obtained by integrating over t, i.e.,

$$\begin{aligned} p_{\rm left}(y_2|L) &= \int_0^\infty F_{\rm left}(t')\, dt' \,, \\ \text{and} \quad p_{\rm right}(y_2|L) &= \int_0^\infty F_{\rm right}(t')\, dt' \,. \end{aligned} \tag{46}$$

Hence, if we condition on ending the process by the left boundary, the marginal distribution of the completion time t_ℓ is given by

$$P^{\rm left}_{t_\ell}(t) = \frac{F_{\rm left}(t)}{\int_0^\infty F_{\rm left}(t')\, dt'} = \frac{F_{\rm left}(t)}{p_{\rm left}(y_2|L)} \,. \tag{47}$$

Upon dividing by the constant conditioning factor $p_{\rm left}(y_2|L)$, it then follows that the joint distribution $P^{\rm left}(t_\ell = t, z_2(t) = z)$ can then be read off the first term in Eq. (46), namely,

$$\begin{aligned} & P^{\rm left}(t,z) = \\ & \left[\frac{1}{p_{\rm left}(y_2|L)}\right] (D_1 + D_2)\, \frac{\partial P(z_1, z_2 = z, t)}{\partial z_1}\Big|_{z_1=0} , \end{aligned} \tag{48}$$

so that the marginal distribution of t_ℓ is then given by integrating over z, i.e.,

$$\begin{aligned} & P^{\rm left}_{t_\ell}(t_\ell = t) = \int_0^\infty dz\, P^{\rm left}(t,z) \\ & = \left[\frac{1}{p_{\rm left}(y_2|L)}\right] (D_1 + D_2) \int_0^\infty dz_2\, \frac{\partial P(z_1, z_2, t)}{\partial z_1}\Big|_{z_1=0} , \end{aligned} \tag{49}$$

which precisely coincides with the definition in Eq. (47). Similarly, by integrating over t, one can obtain the other desired marginal

$$\begin{aligned} & P^{\rm left}_z(z_2(t_\ell) = z) = \int_0^\infty dt\, P^{\rm left}(t,z) \\ & = \left[\frac{1}{p_{\rm left}(y_2|L)}\right] (D_1 + D_2) \int_0^\infty dt\, \frac{\partial P(z_1, z, t)}{\partial z_1}\Big|_{z_1=0} . \end{aligned} \tag{50}$$

To solve for $P(z_1, z_2, t)$ in Eq. (42), we again perform the change of variables analogous to Eq. (21),

$$\begin{aligned} w_1 &= \frac{\sqrt{D_0}}{\sqrt{2-\gamma}} \left[\frac{z_1}{\sqrt{D_1 + D_2}} + \frac{z_2}{\sqrt{D_2 + D_3}}\right] \\ w_2 &= \frac{\sqrt{D_0}}{\sqrt{2+\gamma}} \left[-\frac{z_1}{\sqrt{D_1 + D_2}} + \frac{z_2}{\sqrt{D_2 + D_3}}\right] , \end{aligned} \tag{51}$$

where γ is given in Eq. (22) and D_0 is kept arbitrary as in Eq. (21). The specific value of D_0 is not important, it is introduced so that w_1 and w_2 have the dimensions of length. Let $\tilde{P}(w_1, w_2, t)$ denote the probability density in the (w_1, w_2) coordinates which is simply related to $P(z_1, z_2, t)$ via a constant Jacobian factor

$$\begin{aligned} P(z_1, z_2, t) &= J\, \tilde{P}(w_1, w_2, t) \quad \text{where} \\ J &= \frac{D_0}{\sqrt{D_1\, D_2 + D_2\, D_3 + D_3\, D_1}} \,. \end{aligned} \tag{52}$$

Then $\tilde{P}(w_1, w_2, t)$ satisfies the two-dimensional diffusion equation

$$\frac{\partial \tilde{P}}{\partial t} = D_0 \left[\frac{\partial^2 \tilde{P}}{\partial w_1^2} + \frac{\partial^2 \tilde{P}}{\partial w_2^2}\right] \tag{53}$$

within a wedge in the (w_1, w_2) plane that is bounded by the two lines $w_2 = \pm \tan(\alpha)\, w_1$ (see Fig. 5), with α defined in Eq. (24). The boundary conditions are absorbing on the two bounding lines, i.e., $\tilde{P}(w_1, w_2, t) = 0$ when $w_2 = \pm \tan(\alpha)\, w_1$. Similarly, the initial condition (43) also transforms accordingly in the (w_1, w_2) coordinates.

The general solution of the diffusion equation in a wedge with absorbing boundary conditions can be easily obtained in the polar coordinates $(w_1, w_2) \to (r, \phi)$ where

$$r = \sqrt{w_1^2 + w_2^2}\,; \quad \text{and} \quad \phi = \tan^{-1}\left(\frac{w_2}{w_1}\right) . \tag{54}$$

The explicit solution can be obtained by the method of separation of variables. The solution reads

$$\tilde{P}(r, \phi, t) = \frac{1}{\alpha_W\, D_0\, t} \sum_{n=1}^\infty \sin\left(\frac{n\pi(\alpha + \phi)}{\alpha_W}\right) \sin\left(\frac{n\pi(\alpha + \phi_0)}{\alpha_W}\right) e^{-(r^2 + r_0^2)/4 D_0 t}\, I_{n\pi/\alpha_W}\left(\frac{r\, r_0}{2\, D_0\, t}\right) , \tag{55}$$

where $\alpha_W = 2\alpha$ is the wedge angle and $I_\nu(z)$ is the modified Bessel function of the first kind with index ν and

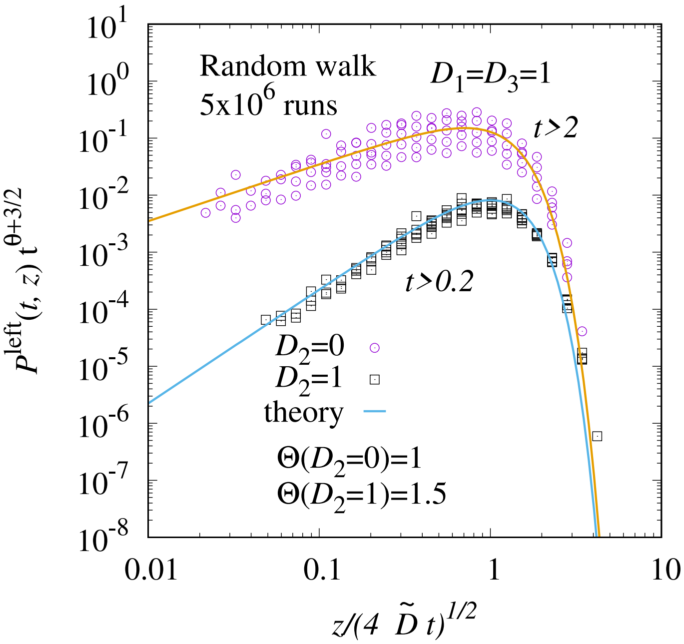

FIG. 9. Theoretical predictions for the scaling behavior of the joint distribution $P^{\rm left}(t,z)$ in Eqs. (61)-(62) shown by solid lines for two values of t are compared with numerical simulations (symbols). In the simulation we fixed $D_1 = D_3 = 1$ and considered two values of $D_2 = 0$ and $D_2 = 1$. In these cases, the theoretical predictions of the exponent θ in Eq. (59) are respectively $\theta = 1$ (for $D_2 = 0$) and $\theta = 3/2$ (for $D_2 = 1$).

argument z. Here (r_0, ϕ_0) refers to the initial condition from where the diffusing particle starts. One can then express the solution $\tilde{P}(w_1, w_2, t)$ in cartesian coordinates (w_1, w_2) by using the transformation in (54). Substituting this general solution $\tilde{P}(w_1, w_2, t)$ in (53) then yields the full exact solution $P(z_1, z_2, t)$ at all times t. Also, using this full solution in Eq. (48), one can then, in principle, compute the joint distribution $P^{\rm left}(t,z)$ for all t and all z. However, this calculation is rather cumbersome and it is more interesting to extract the asymptotic behavior of $P^{\rm left}(t,z)$ for large t and large z. In fact, as we will see below, there is a scaling regime with $t \to \infty$, $z \to \infty$ but with the ratio $z/\sqrt{t}$ fixed, where the expression of $P^{\rm left}(t,z)$ takes a particularly simple explicit form. To derive this scaling behavior for large t and large z, we need to first extract the behavior of $P(z_1, z_2, t)$ for large t (and large z_2 and $z_1 \to 0$) from the general exact solution (55) and then use it in Eq. (48) to compute the scaling behavior $P^{\rm left}(t,z)$. This is presented in the subsection below.

A. Asymptotic large-t behavior of $P^{\rm left}(z,t)$

To analyze the large-t behavior of $P(z_1, z_2, t)$, we start from the general solution (55) in polar coordinates. We will now consider the scaling limit when $t \to \infty$, $r \to \infty$ with the ratio $r/\sqrt{t}$ fixed. We keep $r_0 \sim O(1)$ fixed. We will also use the following asymptotic behavior of $I_\nu(z)$

$$I_\nu(z) \approx \frac{2^{-\nu}}{\Gamma(1+\nu)}\, z^\nu \quad \text{as} \quad z \to 0\,. \tag{56}$$

From (55), we see that in the scaling regime when $r \sim \sqrt{t} \gg 1$ with $r_0 \sim O(1)$, the argument $r r_0/(2D_0 t)$ of the Bessel function becomes small. Hence, we can use the asymptotic behavior in (56). This shows that the dominant contribution to the sum in Eq. (55) comes from the $n = 1$ term, leading to (after slight rearrangements)

$$\tilde{P}(r,\phi,t) \approx \tag{57}$$
$$\frac{A\, r_0^{2\theta}}{(D_0\, t)^{\theta+1}} \sin\left(\frac{\pi(\alpha+\phi)}{\alpha_W}\right) e^{-r^2/4D_0 t} \left(\frac{r^2}{4\, D_0\, t}\right)^{\theta},$$

where A is an unimportant dimensionless constant dependent on the initial condition (and can be absorbed in the overall normalization constant) and the exponent θ is given by

$$\begin{aligned} \theta &= \frac{\pi}{2\,\alpha_W} \quad \text{where} \\ \alpha_W &= 2\,\tan^{-1}\left(\sqrt{\frac{2-\gamma}{2+\gamma}}\right) = \cos^{-1}\left(\frac{\gamma}{2}\right). \end{aligned} \tag{58}$$

Using the expression for γ in (22), the exponent θ reads explicitly

$$\theta = \frac{\pi}{2\cos^{-1}\left(\frac{D_2}{\sqrt{(D_1+D_2)(D_2+D_3)}}\right)}\,, \tag{59}$$

and thus depends continuously on the diffusion constants $\{D_1, D_2, D_3\}$. In fact, integrating (58) over all space and using (53), it is clear that the survial probability in (44) decays as a power law at late times

$$S(t) = J \int_{-\alpha}^{\alpha} d\phi \int_0^\infty r\, dr\, \tilde{P}(r,\phi,t) \sim \frac{B_1}{t^\theta}\,, \tag{60}$$

where B_1 is a computable constant independent of t. The exponent θ is called the persistence exponent [53] and its exact expression $\theta = \pi/(2\alpha_W)$ in the wedge geometry is well-known in the literature [16, 53].

Next, we want to compute the joint distribution $P^{\rm left}(t,z)$ in Eq. (48), by taking the derivative of Eq. (58) with respect to z_1 and taking the limit $z_1 \to 0$. Note that for ϕ and r^2 in (58) are both functions of z_1. Hence one needs to derive both ϕ and r^2 with respect to z_1 and take the limit $z_1 \to 0$. It is however easy to show that the leading contribution for large t arises from the derivative of the term $\sin\left(\frac{\pi(\alpha+\phi)}{\alpha_W}\right)$ with respect to z_1 as $z_1 \to 0$ in Eq. (58). We skip the boring alegebraic details here and present only the final result. We find that in the scaling limit $t \to \infty$, $z_2 = z \to \infty$ but with

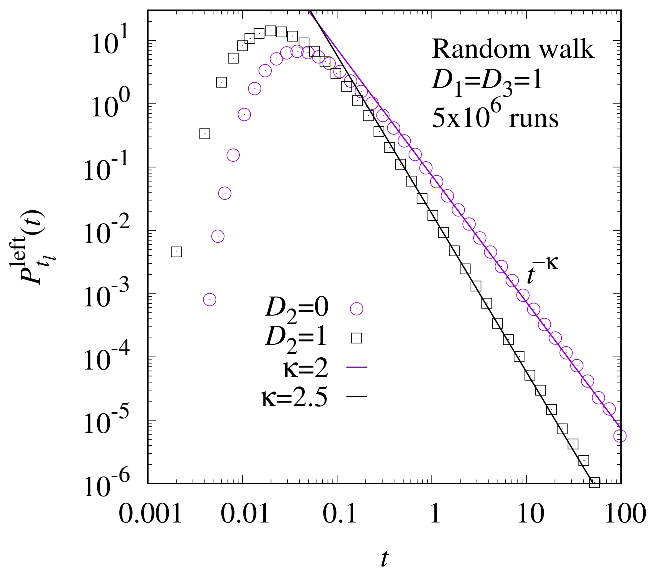

FIG. 10. Theoretical prediction for the power law decay of the marginal distribution $P^{\rm left}_{t_\ell}(t) \sim t^{-\kappa}$ in Eq. (63) as a function of t (solid lines) is compared with numerical simulations (symbols), where only "large" splitting times $t > 2$ habe been considered. In the simulation we fixed $D_1 = D_3 = 1$ and considered two values of $D_2 = 0$ and $D_2 = 1$. The theoretical predictions of the exponent κ in Eq. (64) in these cases are respectively $\kappa = 2$ (for $D_2 = 0$) and $\kappa = 5/2$ (for $D_2 = 1$). The agreement between theoretical predictions and simulations is excellent.

the ratio $z/\sqrt{t}$ fixed, the joint distribution $P^{\rm left}(t,z)$, to leading order for large t, approaches a scaling form

$$P^{\rm left}(t,z) \;\approx\; \frac{C}{t^{\theta+3/2}}\, H\left(\frac{z}{\sqrt{4\,\tilde{D}\,t}}\right) , \qquad (61)$$
$$\text{with} \quad \tilde{D} \;=\; \frac{D_1\,D_2 + D_2\,D_3 + D_3\,D_1}{D_1 + D_2} \, .$$

Here, C is an overall constant (that depends on initial separations y_1 and y_2), θ is the persistence exponent given in (59)) and the exact scaling function $H(u)$ is given by

$$H(u) = u^{2\theta-1}\, e^{-u^2} \quad \text{for} \quad u \geq 0 \, . \qquad (62)$$

In Fig. 9, we compare this theoretical prediction to numerical simulations. Here we used $t_{\rm max} = 100$ and $\Delta t = 10^{-4}$ to obtain a good statistics in reasonable time. Since we rescale the data for different values of z and t, the resulting data points exhibit a considerable scatter, but overall a very good agreement between numerics and theory is visible.

Having obtained the scaling form (61) of the joint distribution $P^{\rm left}(t,z)$, one can easily derive the tails of the marginal distributions $P^{\rm left}_{t_\ell}(t)$ (by integrating over z) and $P^{\rm left}(z)$ (by integrating over t). The former is given by

$$P^{\rm left}_{t_\ell}(t) \;=\; \int_0^\infty P^{\rm left}(t,z)\,dz \approx \frac{C_1}{t^\kappa} \quad \text{as} \quad t \to \infty \, ,$$
$$\text{with} \quad \kappa = \theta + 1 \, , \qquad (63)$$

where the amplitude C_1 of the power law tail can be easily computed in terms of C in Eq. (61) and the exponent θ is given in Eq. (59). Using the expression for θ in Eq. (59), one can express the exponent κ as

$$\kappa = 1 + \frac{\pi}{2\,\cos^{-1}\left(\frac{D_2}{\sqrt{(D_1+D_2)(D_2+D_3)}}\right)} \, . \qquad (64)$$

This result in Eq. (63) is clearly consistent with the fact that the survival probability $S(t) \sim t^{-\theta}$ as $t \to \infty$ (see (60)). Hence, the total first-passage probability (through the left as well as the right boundary) $F(t) = -dS/dt$ defined in Eq. (46) decays as $F(t) \sim t^{-\theta-1}$ as $t \to \infty$. Naturally, one would then expect that the first-passage probability density through the left boundary $F_{\rm left}(t)$, defined in Eq. (46), also decays as a power law with the same exponent $\theta + 1$. Now, the marginal distribution $P^{\rm left}_{t_\ell}(t)$ is just the conditional first-passage time density through the left boundary and hence is proportional to $F_{\rm left}(t)$, as in Eq. (47). Hence, the power law decay in Eq. (63) at late times is perfectly consistent with this observation. In Fig. 10, we present numerical simulations to compare with the theoretical prediction in (63).

Similarly, the marginal distribution $P^{\rm left}_z(z)$, obtained by integrating (61) over t, also decays as a power law for large z

$$P^{\rm left}_z(z) \;=\; \int_0^\infty P^{\rm left}(t,z)\,dt \approx \frac{C_2}{z^\beta} \quad \text{as} \quad z \to \infty \, , \qquad (65)$$
$$\text{where} \quad \beta = 2\theta + 1 \, .$$

The amplitude C_2 is again simply related to C in Eq. (61). Using the expression for θ in (59), one can express the exponent β as

$$\beta = 2\theta + 1 \;=\; 1 + \frac{\pi}{\cos^{-1}\left(\frac{\gamma}{2}\right)} \qquad (66)$$
$$\;=\; 1 + \frac{\pi}{\cos^{-1}\left(\frac{D_2}{\sqrt{(D_1+D_2)(D_2+D_3)}}\right)} \, ,$$

which depends continuously on the diffusion constants D_1, D_2 and D_3. For example, in the case $D_1 = D_2 = D_3$, we get $\beta = 4$ from (66). In contrast, for $D_2 = 0$, we get $\beta = 3$. We also verified these large z theoretical predictions in our numerical simulations finding excellent agreement (see Fig. 11).

V. GENERALIZATION TO FRACTIONAL BROWNIAN MOTION

We next study a generalization of our three-paricle model where the two outer walkers with positions $x_1(t)$

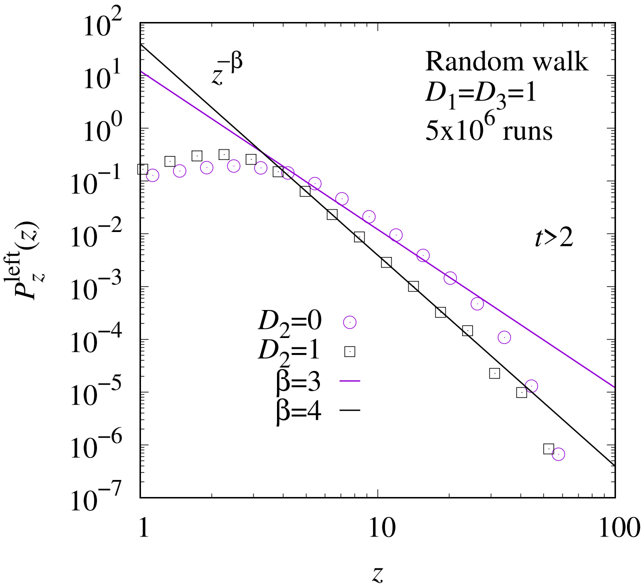

FIG. 11. Theoretical prediction for the power law decay of the marginal distribution $P_z^{\rm left}(z) \sim z^{-\beta}$ in Eq. (65) as a function of z (solid lines) is compared with numerical simulations (symbols). In the simulation we fixed $D_1 = D_3 = 1$ and considered two values of $D_2 = 0$ and $D_2 = 1$ and excluded small splitting times $t \leq 2$. The theoretical predictions of the exponent β in Eq. (66) in these cases are respectively $\beta = 3$ (for $D_2 = 0$) and $\beta = 4$ (for $D_2 = 1$). The agreement between theoretical predictions and simulations is excellent.

and $x_3(t)$ perform ordinary Brownian motions with diffusion constants D_1 and D_3 as before, but the central walker $x_2(t)$ performs a fractional Brownian motion (fBM). In the context of the translocation process, this means that the polymerization and depolymerizatiom of single monomers at the chain ends on both sides are modeled by a standard random walker (or Brownian motion in the continuum), whereas the actual translocation through the pore is modeled by an fBM. As mentioned in the introduction, the fBM is a Gaussian process with zero mean and a correlator given by [11]

$$\langle x_2(t_1)\, x_2(t_2)\rangle = D_2(|t_2|^{2H} + |t_2|^{2H} - |t_2 - t_1|^{2H}) \,, \quad (67)$$

with Hurst exponent $0 < H < 1$. This leads to a mean-squared displacement (msd) of

$$\langle (x_2(t_0 + t) - x_2(t_0))^2\rangle = 2D_2 t^{2H} \,. \quad (68)$$

Thus, for $H = 1/2$, one recovers the standard Brownian motion. For $H < 1/2$, the long-time behavior of the walk is subdiffusive, i.e., slower as compared to the $H = 1/2$ case, whereas on short time scales $t < 1$ it is faster. For $H > 1/2$, the opposite behavior is observed. Furthermore, for $H = 1/2$, the process is Markovian, while for $H \neq 1/2$ it is non-Markovian [12, 13]. Owing to the non-Markovian nature of the process for $H \neq 1/2$, it is hard to compute analytically the splitting probability as well as the distribution of the time of translocation and that of the chain length at the time of translocation. Hence we compute these observables numerically for $H \neq 1/2$.

To treat the walk numerically, we again consider discrete time steps Δt. The temporal correlations of the position arise from correlations between successive increments $\Delta x_2(t) = x_2(t + \Delta t) - x_2(t)$. The correlation $\langle \Delta x_2(t)\, \Delta x_2(t + t')\rangle$ between two increments evaluates for $D_2 = 1$ as $|t' + \Delta t|^{2H} + |t' - \Delta t|^{2H} - 2|t'|^{2H}$, which is for $H = 1/2$ zero for all values of $t' \geq \Delta t$, as expected, but non-zero for other values of H.

Technically, to generate a realization of a correlated walks, we first generate correlated Gaussian increments $\tilde{\xi}(k)$ for unit step size $\Delta t = 1$, i.e., at times $k = 1, 2, \ldots$, following correlation Eq. (67). This we achieve efficiently following the Davies-Harte approach [57] which is based on Fast Fourier Transform, details can be found in the literature [14]. From these unit step increments $\tilde{\xi}(k)$ we obtain the actual walks, in generalization of Eq. (15), as

$$x_2((k + 1)\Delta t) = x_2(k\Delta t) + \sqrt{2D}(\Delta t)^H \tilde{\xi}(k) \,. \quad (69)$$

In Fig. 12 we show the numerically obtained hitting probability $p_{\rm left}(y_2|L)$ as a function of y_2 for $L = 1$ and the cases $H = 0.25$, and $H = 0.75$, compared to the uncorrelated case $H = 0.5$ as studied above. The upper panel shows the result for $D_1 = D_2 = D_3 = 1$. For $H = 0.25$, the deviation from the linear behavior $p_{\rm left}(y_2|L) = y_2$ is more pronounced than for the uncorrelated case. Nevertheless, since the diffusion constant is rather large in comparison with the initial wall distance $L = 1$, the typical splitting times are relatively short. Consequently, the observed behavior mainly reflects the short-time dynamics..

Thus, we have also considered the case $D_1 = D_2 = D_3 = 0.02$ with still $L = 1$. This changes both the temporal correlations (for $H \neq 1/2$) and the mean-square displacement. The particles move more slowly, so it takes longer for the middle walker to hit a boundary. Note that alternatively we could have also increased L. Accordingly, we have used $t_{\max} = 100$, with still $\Delta t = 10^{-5}$, so that, in more than 99% of the realizations, the middle walker hits either the left or right boundary. As visible in the figure, the behavior for $H = 0.75$ changes considerably, while for $H = 0.25$ the result is still similar to the medium-diffusion case. In general, the latter result is qualitatively similar to the behavior that has been found for the case of fractional Brownian motion with fixed boundaries [20].

In Fig. 13 we show the distribution $P_{t_\ell}^{\rm left}(t)$ of splitting times for the two cases $H = 0.25$ and $H = 0.75$, and compared them with the previous result for the uncorrelated case $H = 0.5$. Again, to obtain good statistics within a reasonable computation time, much larger than for the splitting probability, we used $t_{\max} = 100$ and $\Delta t = 10^{-4}$. In the upper plot, we consider the case $D_1 = D_2 = D_3 = 1$. The mean-squared displacement given by Eq. (68) for time $t = 1$ is always $2D_i = 2$ in our model, which is here already of the order of $L = 1$. Since for small times $t < 1$, the msd is larger for small

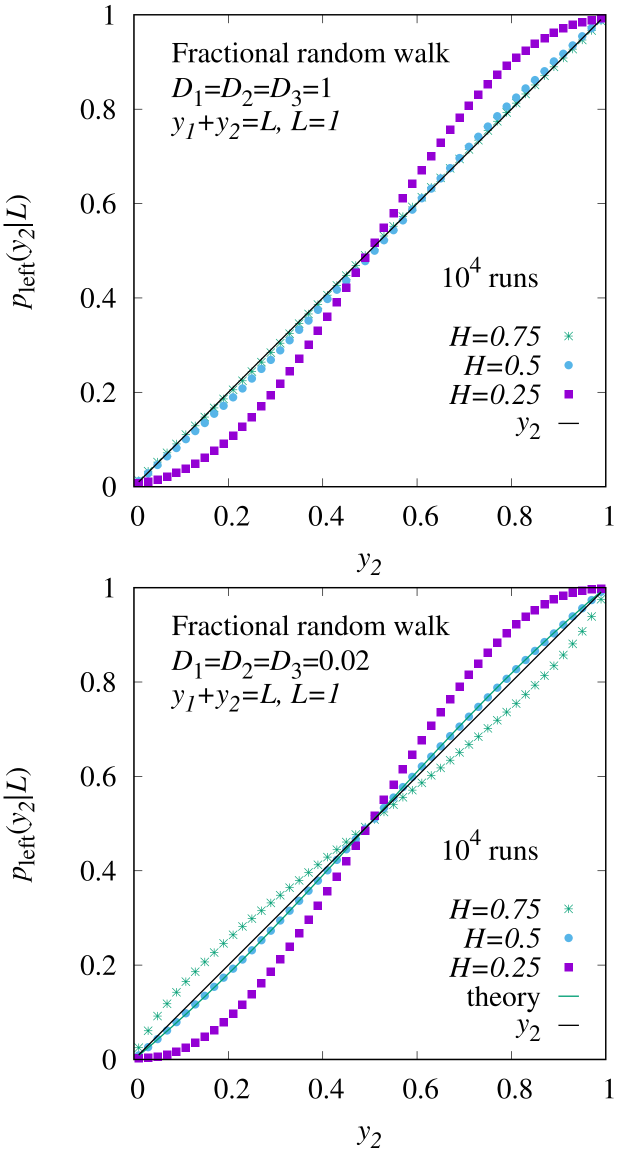

FIG. 12. The numerically obtained splitting probability $p_{\rm left}(y_2|L)$ as a function of y_2 with $L = 1$ for the cases $H = 0.25$, $H = 0.5$ and $H = 0.75$, with (top) $D_1 = D_2 = D_3 = 1$, $t_{\max} = 10$ and (bottom) $D_1 = D_2 = D_3 = 0.2\, t_{\max=100} = 100$.

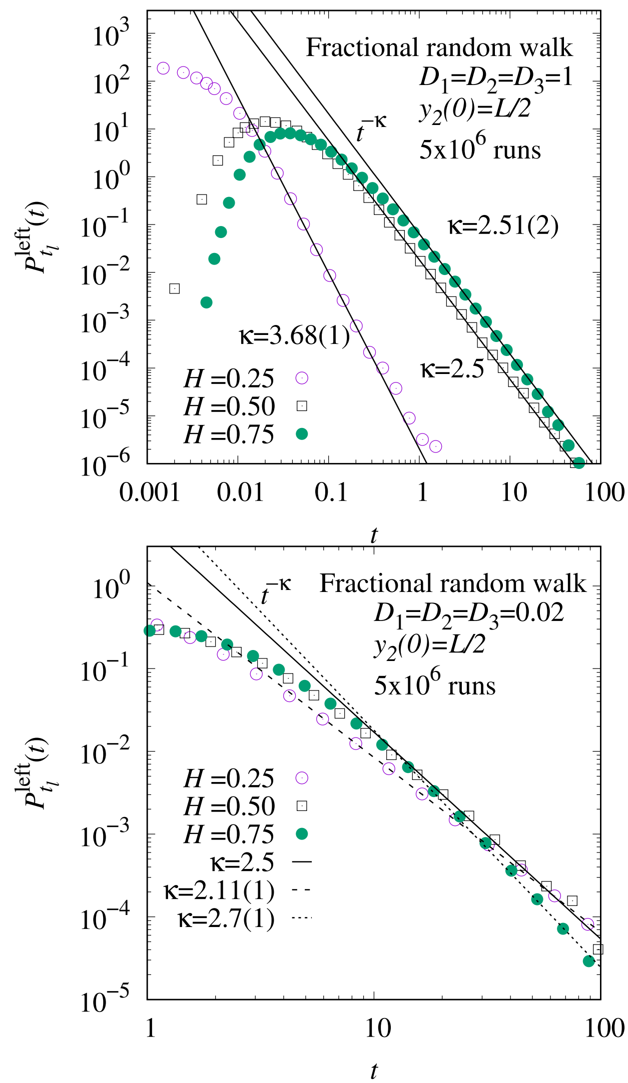

FIG. 13. Marginal distribution $P^{\rm left}_{t_\ell}(t)$ obtained from the numerical simulations for $H = 0.25$, $H = 0.5$ and $H = 0.75$, $L = 1$, and for (top) $D_1 = D_2 = D_3 = 1$ and (bottom) $D_1 = D_2 = D_3 = 0.02$.

values of H as compared to larger values of H, the splitting times t are typically smaller for $H = 0.25$ than for $H = 0.75$, as visible in the figure. The data for $H = 0.25$ is compatible with power law $\sim t^{-\kappa}$ as for the uncorrelated case, but with a numerical value $\kappa = 3.68(2)$ which is corresponding larger than the value $\kappa = 2.5$. Finally, since the msd for $H = 0.75$ is rather small for $t < 1$, the case $H = 0.75$ exhibits larger splitting times. The actual shape of $P^{\rm left}_{t_\ell}(t)$ is very similar to the uncorrelated case, a fit to the middle part yields $\kappa = 2.51(2)$.

For the slower case $D_1 = D_2 = D_3 = 0.02$ the results are shown in the bottom of Fig. 13. Here the splitting times are much larger, as expected. Interestingly, for the correlated cases $H \neq 1/2$, we find different exponents $\kappa = 2.11(19$ $(H = 0.25)$ and $\kappa = 2.7(1)$ $(H = 0.75)$ as compared to the case $D_1 = D_2 = D_3 = 1$, while for the uncorrelated case $H = 1/2$ we still observe $\kappa = 5/2$, naturally because only the time scale is affected here, which does not change the distribution of distances upon hitting the boundaries. In general we find the expected long-time behavior comparing the results for different values of H. Namely, for $H = 0.25$ the time distributions decreases in the tail slower than for $H = 0.5$ which itself decreases slower than for $H = 0.75$.

In Fig. 14 we show the distribution $P^{\rm left}_z(z)$ of the separation $z = y_2$ of the middle walker to the right boundary at the moment were the middle walker hits the left boundary, integrated over all splitting times. Here, the three cases $H = 0.25$, $H = 0.5$ and $H = 0.75$ are considered, again for $L = 1$ and $x_2(0) = L/2$.

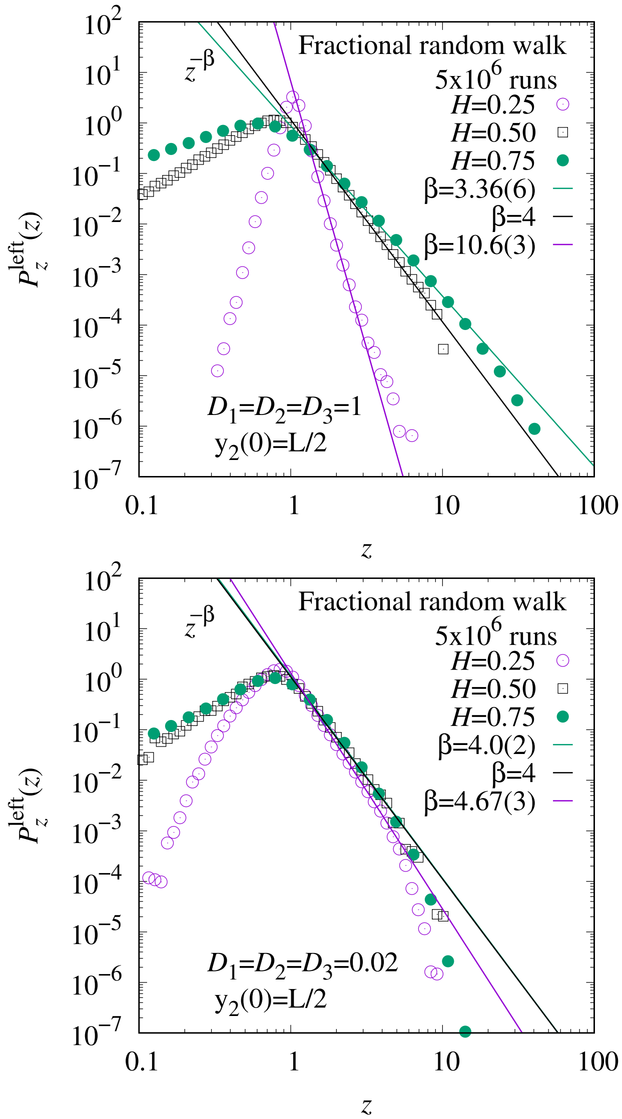

FIG. 14. Distribution $P_z^{\rm left}(z)$ obtained from the numerical simulations for the three cases $H = 0.25$, $H = 0.5$ (uncorrelated) and $H = 0.75$ for $L = 1$. The upper plot is for $D_1 = D_2 = D_3 = 1$ while the lower one for $D_1 = D_2 = D_3 = 0.02$.

First, we discuss the case $D_1 = D_2 = D_3 = 1$, which is shown on the upper part of the figure. We also observe in the right tails a power law-behavior $\sim z^{-\beta}$ like for the uncorrelated case at larger times. But since the behavior for $H = 0.25$ is dominated by very small splitting times, see Fig. 13, the two boundaries x_1 and x_3 have not moved much, so the distance of the two boundaries is near the initial distance $L = 1$, such that the separation y_2 between the middle walker and the right boundary is also near $L = 1$. Thus, the distribution falls off very quickly, which is compatible with a power law with exponent $\beta = 10.6(3)$ obtained from the fit. The dominance of the distance $y_2 = 1$ is also visible for $H = 0.5$ and $H = 0.75$ but here larger splitting times and correspondingly larger distances y_2 appear, reflected by less steep tails. For $H = 0.75$, we observe a slightly smaller exponent than the exact value $\beta = 4$ which holds for the uncorrelated case.

On the lower panel of Fig. 14, we display the corresponding results for the slow behavior $D_1 = D_2 = D_3 = 0.02$ which leads to larger splitting times, as discussed. The data for the uncorrelated case does not change as compared to the case $D_i = 1$, except for statistical fluctuations, since changing all diffusion constants by the same factor only changes the clock speed for the uncorrelated case. Thus, there is no change of the exponent β in Eq. (66). Now the distributions of distances for the three cases are very similar to each other, as can already be expected from the previously discussed distributions of splitting times. From power-law fits in Eq. (65), we obtain $\beta = 4.67(3)$ for $H = 0.25$ and $\beta = 4.0(2)$ for $H = 0.75$, the latter one being compatible with the known value $\beta = 4$ for the uncorrelated case.

To summarize, when the central particle performs fBM with Hurst exponent $0 < H < 1$ and the two outer particles perform ordinary Brownian motions with diffusion constants D_1 and D_3, the general features of the splitting probability as well as the two marginals $P_{t_\ell}^{\rm left}(t)$ and $P_z^{\rm left}(z)$ are similar to the case when the central particle performs ordinary Brownian motion ($H = 1/2$). However, the details are different. For example, both the marginal distributions decay as power laws, but the associated exponents β and κ both now depend on H, in addition to depending on the diffusion constants. Thus, although the qualitative behavior remains similar to the Brownian case ($H = 1/2$), the quantitative results depend on the Hurst exponent H.

VI. CONCLUSION

In this work, we studied the translocation process of a polymer chain through a nanopore, where the chain length fluctuates due to the stochastic polymerization-depolymerization at the chain ends. For the case where the translocation process is modelled by a simple Brownain motion, we mapped this process to a problem of three vicious Brownian walkers on a line with different diffusion constants D_1, D_2 and D_3. Under this mapping, the translocation process terminates when the central walker meets any one of the two outer walkers. We computed exactly three important observables: (i) the splitting probability, i.e., the probability that the central walker meets the walker on its left (right) before that on the right (left). In the language of translocation, this splitting probability is the same as the probability that the chain translocates to the right (left) of the pore. (ii) the probability distribution of the time at which the translocation process terminates and (iii) the probability distribution of the length of the polymer chain at the time when the translocation process terminates. We showed that the splitting probability is rather nontrivial in the case when the two outer particles diffuse, compared to the classical well-known case when the two outer particles are fixed (the latter corresponds to the case where there is no polymerization-depolymerization at the chain ends and hence the chain length is fixed). We also showed that the distribution of the translocation time and that of the chain length at the completion time of translocation both have power-law tails with exponents that depend cotinuously on the three diffusion constants D_1, D_2 and D_3. All analytical predictions were validated by extensive numerical simulations, showing excellent agreement over the entire parameter range investigated.

Finally, we extended the model by replacing the Brownian motion of the pore with fractional Brownian motion while keeping the polymer ends diffusive. Owing to the non-Markovian nature of fractional Brownian motion, an analytical treatment is considerably more challenging, and we therefore relied on numerical simulations. We found that the qualitative features of the Brownian case remain robust, while the splitting probabilities and the asymptotic exponents depend continuously on the Hurst exponent. In particular, the persistence exponent and the exponent governing the distribution of the final polymer length vary systematically with the degree of temporal correlations introduced by the fractional Brownian motion.

The present work provides a unified framework for studying first-passage phenomena in systems with fluctuating boundaries and establishes several exact results for Brownian dynamics together with numerical results for their fractional Brownian generalization. Beyond the polymer translocation problem that motivated this study, the methods developed here may be applicable to a broader class of first-passage problems involving moving boundaries or multiple interacting stochastic processes. An interesting direction for future work would be to develop an analytical treatment of the fractional Brownian case and to investigate more realistic models that incorporate interactions, external driving forces, or additional internal degrees of freedom of the polymer.

ACKNOWLEDGMENTS

SNM acknowledges support from ANR Grant No. ANR- 23- CE30-0020-01 EDIPS and the Alexander von Humboldt foundation for the Gay Lussac-Humboldt prize that allowed a visit to the Physics department at Oldenburg University, Germany where part of this work was performed. The simulations were performed at the HPC cluster ROSA, located at the University of Oldenburg (Germany) and funded by the DFG through its Major Research Instrumentation Program (INST 184/225-1 FUGG) and the Ministry of Science and Culture (MWK) of the Lower Saxony State.

[1] J. J. Kasianowicz, E. Brandin, D. Branton, D. W. Deamer, *Characterization of individual polynucleotide molecules using a membrane channel*, Proc. Natl. Acad. Sci. U.S.A. **93**, 13770 (1996).

[2] A. Meller, L. Nivon, D. Branton, *Voltage-driven DNA translocations through a nanopore*, Phys. Rev. Lett. **86**, 3435 (2001).

[3] A. Meller, *Dynamics of polynucleotide transport through nanometre-scale pores*, J. Phys. Condens. Matter **15**, R581 (2003).

[4] A. Yu. Grosberg, S. Nechaev, M. Tamm, O. Vasilyev, *How long does it take to pull an ideal polymer into a small hole?*, Phys. Rev. Lett. **96**, 228105 (2006).

[5] M. Muthukumar, *Polymer translocation through a hole*, J. Chem. Phys. **111**, 10371 (1999).

[6] D. K. Lubensky, D. R. Nelson, *Driven polymer translocation through a narrow pore*, Biophys. J. **77**, 1824 (1999).

[7] A. J. Storm, C. Storm, J. Chen, H. Zandbergen, J.-F. Joanny, C. Dekker, *Fast DNA translocation through a solid-state nanopore*, Nano Lett. **5**, 1193 (2005).

[8] J. Chuang, Y. Kantor, M. Kardar, *Anomalous dynamics of translocation*, Phys. Rev. E **65**, 011802 (2001).

[9] Y. Kantor, M. Kardar, *Anomalous dynamics of forced translocation*, Phys. Rev. E **69**, 021806 (2004).

[10] C. Chatelain, Y. Kantor, M. Kardar, *Probability distributions for polymer translocation*, Phys. Rev. E **78**, 021129 (2008).

[11] B. B. Mandelbrot, J. W. van Ness, *Fractional Brownian motions, fractional noises and applications*, SIAM Rev. **10**, 422 (1968).

[12] J. Krug, H. Kallabis, S.N. Majumdar, S.J. Cornell, A.J. Bray, C. Sire, *Persistence Exponents for Fluctuating Interfaces*, Phys. Rev. E ., **56**, 2702 (1997).

[13] K.J. Wiese, S.N. Majumdar, A. Rosso, *Perturbation theory for fractional Brownian motion in presence of absorbing boundaries*, Phys. Rev. E, **83**, 061141 (2011).

[14] A.K. Hartmann, S.N. Majumdar, A. Rosso, *Sampling fractional Brownian motion in presence of absorption: A Markov chain method*, Phys. Rev. E **88**, 022119 (2013).

[15] W. Feller, *An Introduction to Probability Theory and its Appli- cations* (New York, Wiley, 1968).

[16] S. Redner, *A Guide to First-Passage Processes* (Cambridge University Press, Cambridge, 2001).

[17] H. Widom, *Stable processes and integral equations*, Trans. Amer. Math. Soc. **98**, 430 (1961).

[18] R.M. Blumenthal, R.K. Getoor, D.B. Ray, *On the distribution of first hits for the symmetric stable processes*, Trans. Amer. Math. Soc. **99**, 540 (1961).

[19] A. Zoia, A. Rosso, S. N. Majumdar, *Asymptotic behavior of self-affine processes in semi-infinite domains*, Phys. Rev. Lett. **102**, 120602 (2009).

[20] S. N. Majumdar, A. Rosso, A. Zoia, *Hitting Probability for Anomalous Diffusion Processes*, Phys. Rev. Lett. **104**, 020602 (2010).

[21] J. Klinger, R. Voituriez, O. Bénichou, *Splitting probabilities of symmetric jump processes* Phys. Rev. Lett. **129**, 140603 (2022).

[22] M. Guéneau, L. Touzo, *Relating absorbing and hard*

wall boundary conditions for a one-dimensional run-and-tumble particle, J. Phys. A: Math. Theor. **57**, 225005 (2024).

[23] U. Basu, S. N. Majumdar, A. Rosso, *Ergodicity breaking in active run-and-tumble particles in a double-well potential*, APS Open Sci., **1**, 000021 (2026).

[24] D. Frydel, *Forward–backward correspondence between stationary structure and splitting probabilities in active matter*, arXiv: 2606.28709

[25] A. Biswas, S. N. Majumdar, and A. Pal, *Target Search Optimization by Threshold Resetting*, Phys. Rev. Lett. **135**, 227101 (2025).

[26] P.-G. de Gennes, *Scaling Concepts in Polymer Physics* (Cornell University Press, Ithaca, NY, 1979).

[27] G. Odian, *Principles of Polymerization* (John Wiley & Sons, New York, 2004).

[28] J. Wang, T. T. Wang, Z. H. Luo, Y. N. Zhou, *Analytical and numerical simulations of depolymerization based on discrete model: A chain-end scission scenario* AIChE Journal, **69**, 17854 (2023)

[29] A. P. Ribeiro, M. O. Martins, A. O. Figueiras, L. M. Martins, *Introduction to Polymerization and Depolymerization* In *Depolymerization: Concepts, Progress, and Challenges* Vol. 1: Core Concepts and Fundamentals (pp. 1-23). American Chemical Society (2025).

[30] S. Karlin, J. McGregor, *Coincidence probabilities*, Pacific Journal of Mathematics, **9**, 1141 (1959).

[31] P. G. de Gennes, *Soluble model for fibrous structures with steric constraints*, J. Chem. Phys. **48**, 2257 (1968).

[32] M. E. Fisher, *Walks, walls, wetting, and melting*, J. Stat. Phys. **34**, 667 (1984).

[33] D. A. Huse, M. E. Fisher, *Commensurate melting, domain walls, and dislocations*, Phys. Rev. B **29**, 239 (1984).

[34] J. W. Essam, A. J. Guttmann, *Vicious walkers and directed polymer networks in general dimensions*, Phys. Rev. E **52**, 5849 (1995).

[35] C. Krattenthaler, A. J. Guttmann, X. G. Viennot, *Vicious walkers, friendly walkers and Young tableaux: II. With a wall*, J. Phys. A: Math. Gen. **33**, 8835 (2000).

[36] K. Johansson, *Non-intersecting paths, random tilings and random matrices* Probab. Theory Relat. Fields **123**, 225 (2002).

[37] M. Katori, H. Tanemura, *Scaling limit of vicious walks and two-matrix model* Phys. Rev. E, 66, 011105 (2002).

[38] A.J. Bray, K. Winkler, *Vicious walkers in a potential*, J. Phys. A: Math. Gen. **37**, 5493 (2004).

[39] H. L. Richards, T. L. Einstein, *Beyond the Wigner distribution: Schrödinger equations and terrace width distributions*, Phys. Rev. E **72**, 016124 (2005).

[40] C. A. Tracy, H. Widom, *Nonintersecting brownian excursions*, Ann. Appl. Probab., **17**, 953 (2007).

[41] G. Schehr, S. N. Majumdar, A. Comtet, J. Randon-Furling, *Exact Distribution of the Maximal Height of Vicious Walkers*, Phys. Rev. Lett., 101, 150601 (2008).

[42] C. Nadal, S. N. Majumdar, *Nonintersecting Brownian interfaces and Wishart random matrices*, Phys. Rev. E **79**, 061117 (2009).

[43] A. Borodin, P. Ferrari, M. Prahofer, T. Sasamoto, J. Warren, *Maximum of Dyson Brownian motion and non-colliding systems with a boundary*, Electron. Commun. Prob. **14**, 486 (2009).

[44] P.J. Forrester, S.N. Majumdar, G. Schehr, *Non-intersecting Brownian walkers and Yang-Mills theory on the sphere*, Nucl. Phys. B., **844**,500 (2011).

[45] G. Schehr, S.N. Majumdar, A. Comtet, P.J. Forrester, *Reunion probability of N vicious walkers: typical and large fluctuations for large N*, J. Stat. Phys., **150**, 491 (2013).

[46] A. Kundu, S.N. Majumdar, G. Schehr, *Maximal distance travelled by N vicious walkers till their survival* , J. Stat. Phys. **157**, 124 (2014).

[47] G. B. Nguyen, D. Remenik, *Extreme statistics of non-intersecting Brownian paths*, Electron. J. Probab. **22**, (2017).

[48] T. Gautié, P. Le Doussal, S. N. Majumdar, G. Schehr, *Non-crossing Brownian paths and Dyson Brownian motion under a moving boundary*, J. Stat. Phys. 177, 752 (2019).

[49] J. Grela, S. N. Majumdar, G. Schehr, *Non-intersecting Brownian bridges in the flat-to-flat geometry*, J. Stat. Phys. **183**, 1 (2021).

[50] M. E. Fisher, M. P. Gelfand, *The reunions of three dissimilar vicious walkers*, J. Stat. Phys. **53**, 175 (1988).

[51] D. ben Avraham, B. M. Johnson, C. A. Monaco, P. L. Krapivsky, S. Redner, *Ordering of random walks: the leader and the laggard*, J. Phys. A: Math. Gen. **36**, 1789 (2003).

[52] S.N. Majumdar, A.J. Bray, *Maximum Distance Between the Leader and the Laggard for Three Brownian Walkers*, J. Stat. Mech. P08023 (2010).

[53] A. J. Bray, S.N. Majumdar, G. Schehr, *Persistence and first-passage properties in nonequilibrium systems*, Adv. in Phys. **62**, 225 (2013).

[54] S.N. Majumdar, *Brownian Functionals in Physics and Computer Science*, Curr. Sci. **89**, 2076 (2005).

[55] A. K. Hartmann, *Big Practical Guide to Computer Simulations*, (World Scientific, Singapore, 2015)

[56] B. Walter, K. J. Wiese, *Sampling first-passage times of fractional Brownian motion using adaptive bisections*, Phys. Rev. E **101**, 043312 (2020).

[57] R. B. Davies, D. S. Harte, *Test for Hurst effect*, Biometrika **74**, 95 (1987).